US 20220354973A1

(19) **United States**

(12) **Patent Application Publication**

(10) **Pub. No.: US 2022/0354973 A1**

(43) **Pub. Date: Nov. 10, 2022**

Wang et al.

(54) **IRON NITRIDE NANOPARTICLE SUSPENSION**

(71) Applicant: **Regents of the University of Minnesota**, Minneapolis, MN (US)

(72) Inventors: **Jian-Ping Wang**, Shoreview, MN (US); **Kai Wu**, Saint Paul, MN (US); **Bin Ma**, St Paul, MN (US); **Jinming Liu**, Fremont, CA (US)

(21) Appl. No.: **17/659,953**

(22) Filed: **Apr. 20, 2022**

Related U.S. Application Data

(60) Provisional application No. 63/201,246, filed on Apr. 20, 2021.

Publication Classification

(51) **Int. Cl.**

A61K 49/18	(2006.01)
C09C 1/22	(2006.01)
C09C 3/00	(2006.01)
C09C 3/04	(2006.01)
C09C 3/08	(2006.01)
C09C 3/10	(2006.01)

(52) **U.S. Cl.**

CPC ***A61K 49/1854*** (2013.01); ***A61K 49/186*** (2013.01); ***C09C 1/22*** (2013.01); ***C09C 3/006*** (2013.01); ***C09C 3/041*** (2013.01); ***C09C 3/08*** (2013.01); ***C09C 3/10*** (2013.01); *C01P 2004/64* (2013.01); *C01P 2006/42* (2013.01); *B82Y 5/00* (2013.01)

(57) **ABSTRACT**

A method may include wet ball milling a plurality of iron nitride nanoparticles in the presence of a surface active agent to modify a surface of the plurality of iron nitride nanoparticles and form a plurality of surface-modified iron nitride nanoparticles for a variety of biomedical applications and soft magnetic materials related applications.

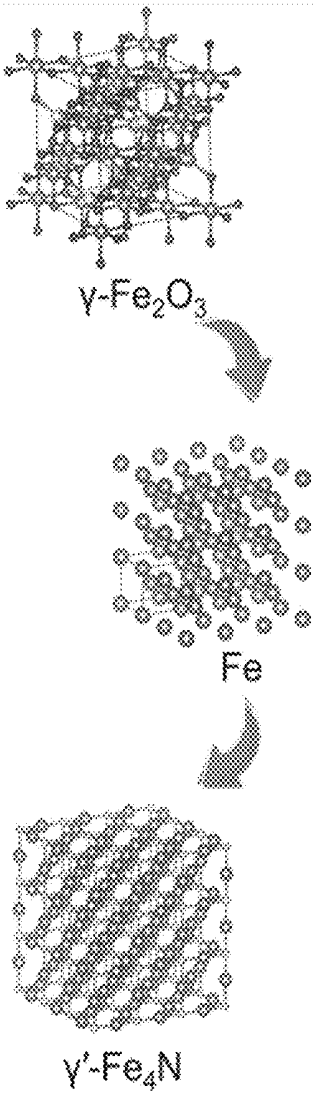

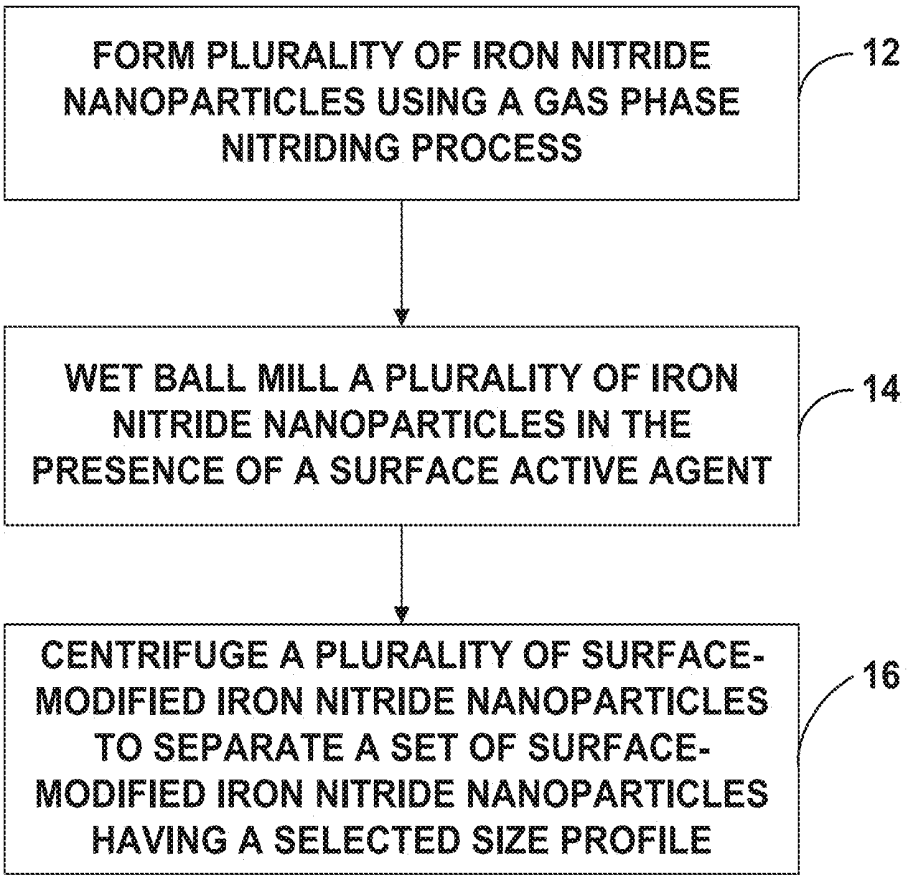
FORM PLURALITY OF IRON NITRIDE NANOPARTICLES USING A GAS PHASE NITRIDING PROCESS
12
WET BALL MILL A PLURALITY OF IRON NITRIDE NANOPARTICLES IN THE PRESENCE OF A SURFACE ACTIVE AGENT
14
CENTRIFUGE A PLURALITY OF SURFACE-MODIFIED IRON NITRIDE NANOPARTICLES TO SEPARATE A SET OF SURFACE-MODIFIED IRON NITRIDE NANOPARTICLES HAVING A SELECTED SIZE PROFILE
16

FIG. 1

FIG. 2A

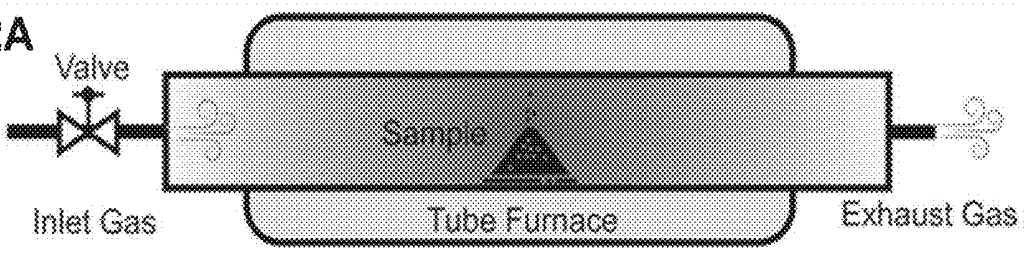

FIG. 2B

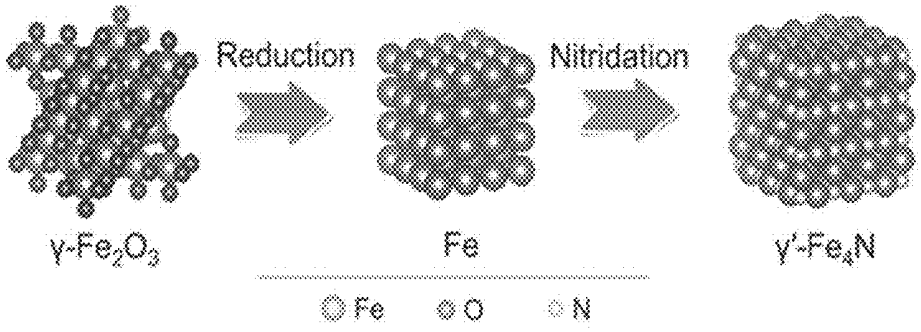

FIG. 2C

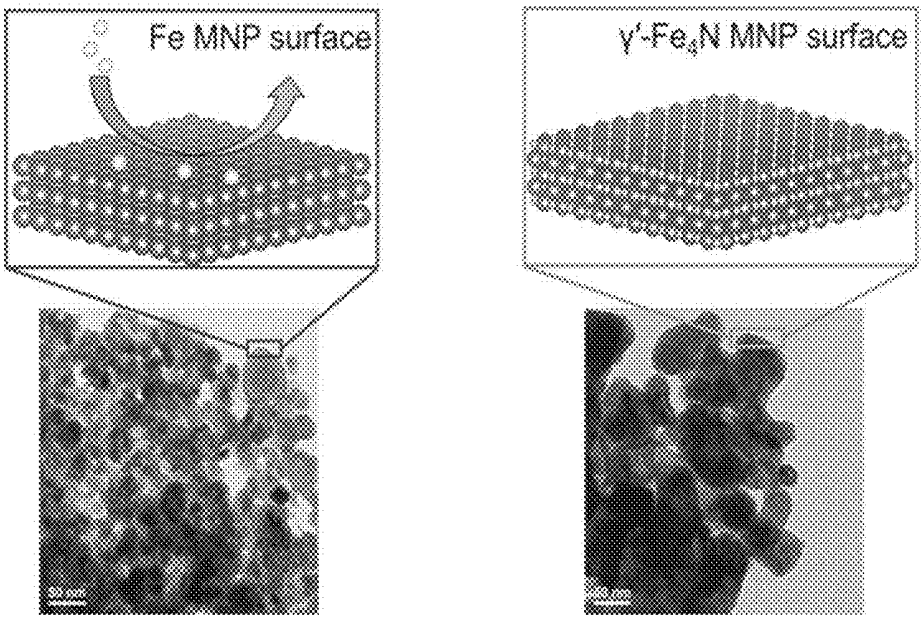

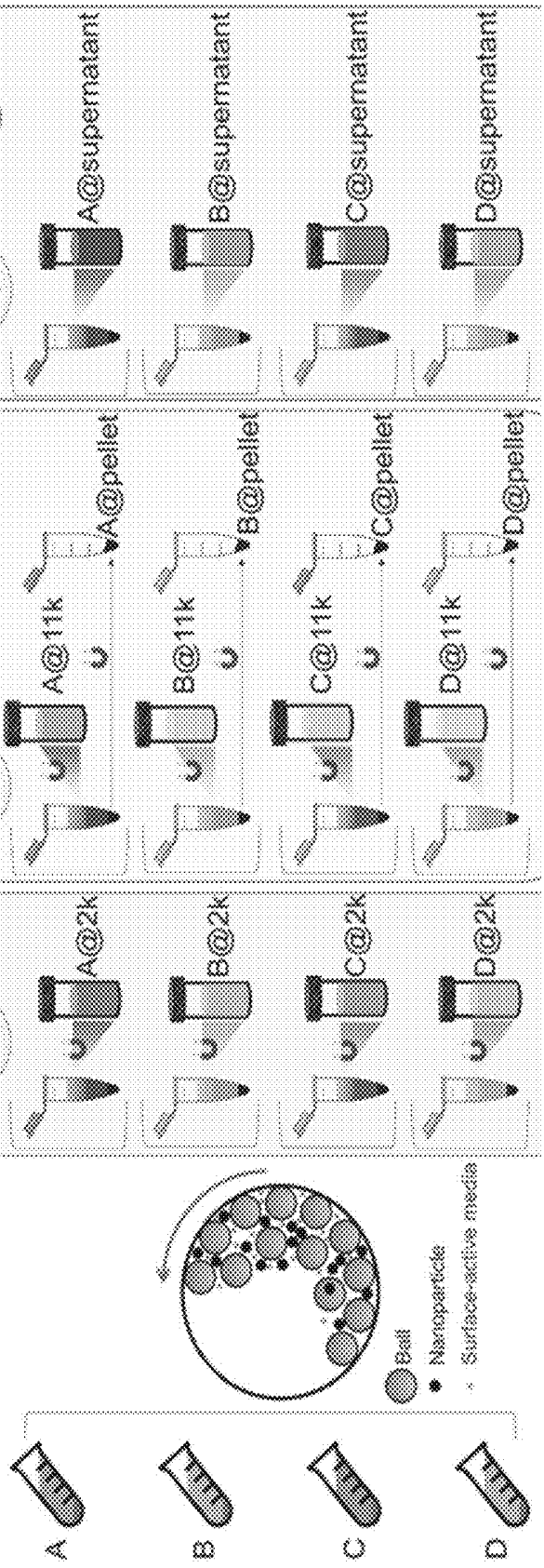

FIG. 3A FIG. 3B FIG. 3C FIG. 3D FIG. 3E

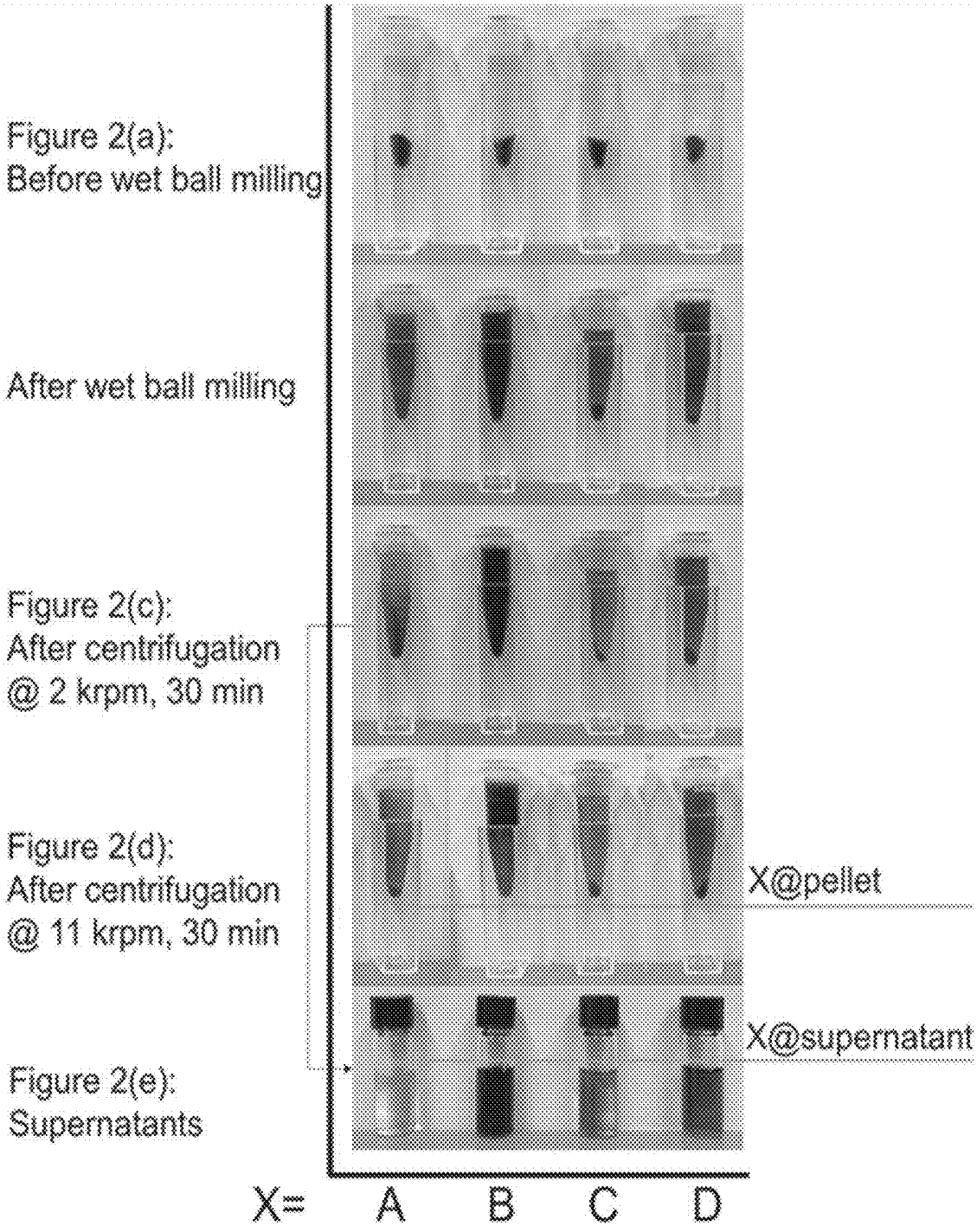
Figure 2(a):
Before wet ball milling
After wet ball milling
Figure 2(c):
After centrifugation
@ 2 krpm, 30 min
Figure 2(d):
After centrifugation
@ 11 krpm, 30 min
Figure 2(e):
Supernatants
X@pellet
X@supernatant
X=
A
B
C
D

FIG. 4

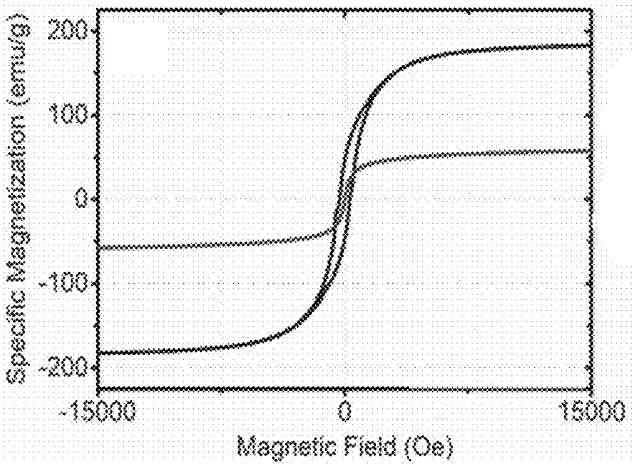

FIG. 5A

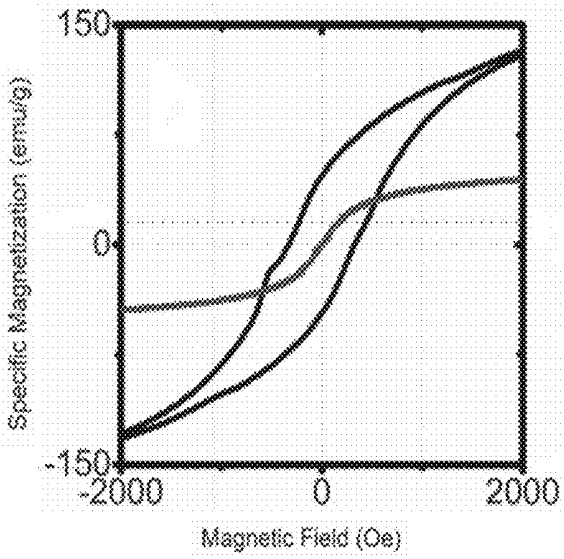

FIG. 5B

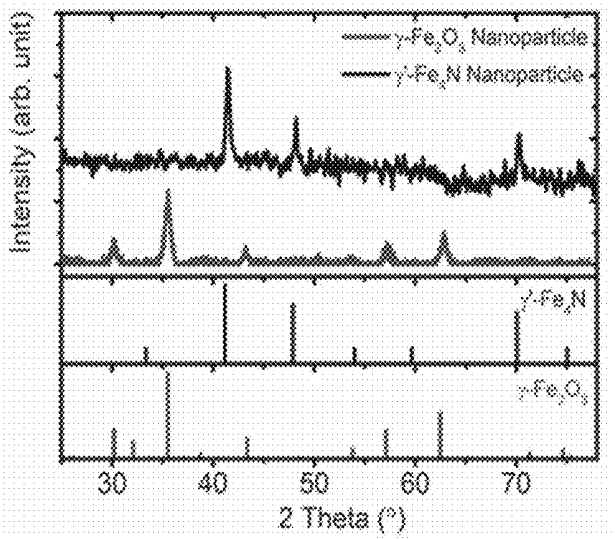

FIG. 5C

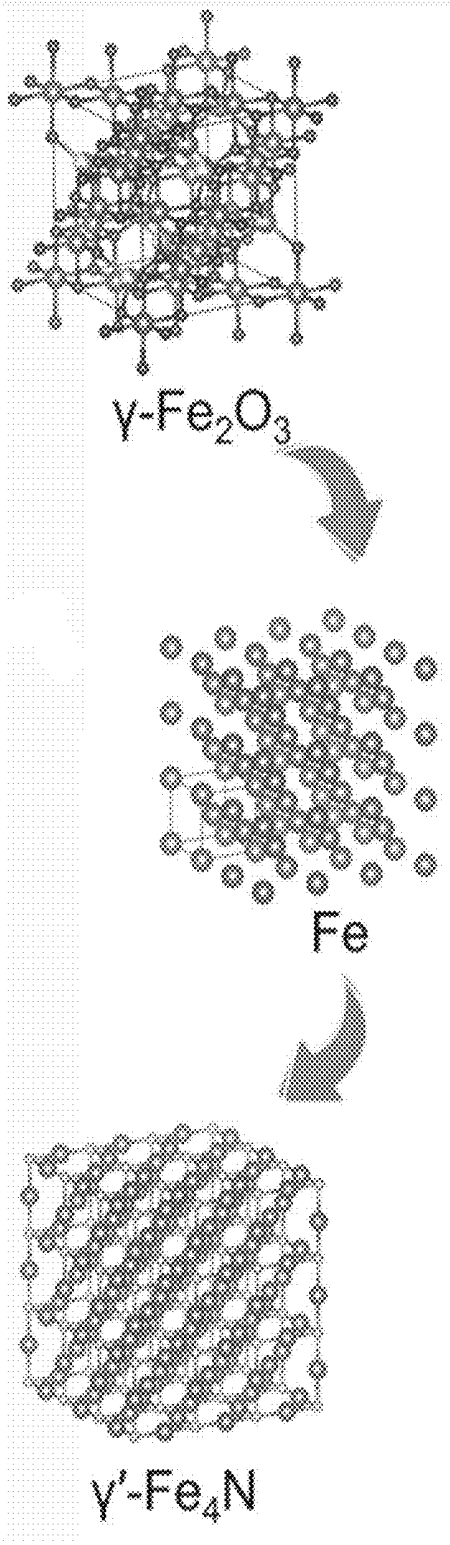

FIG. 5D

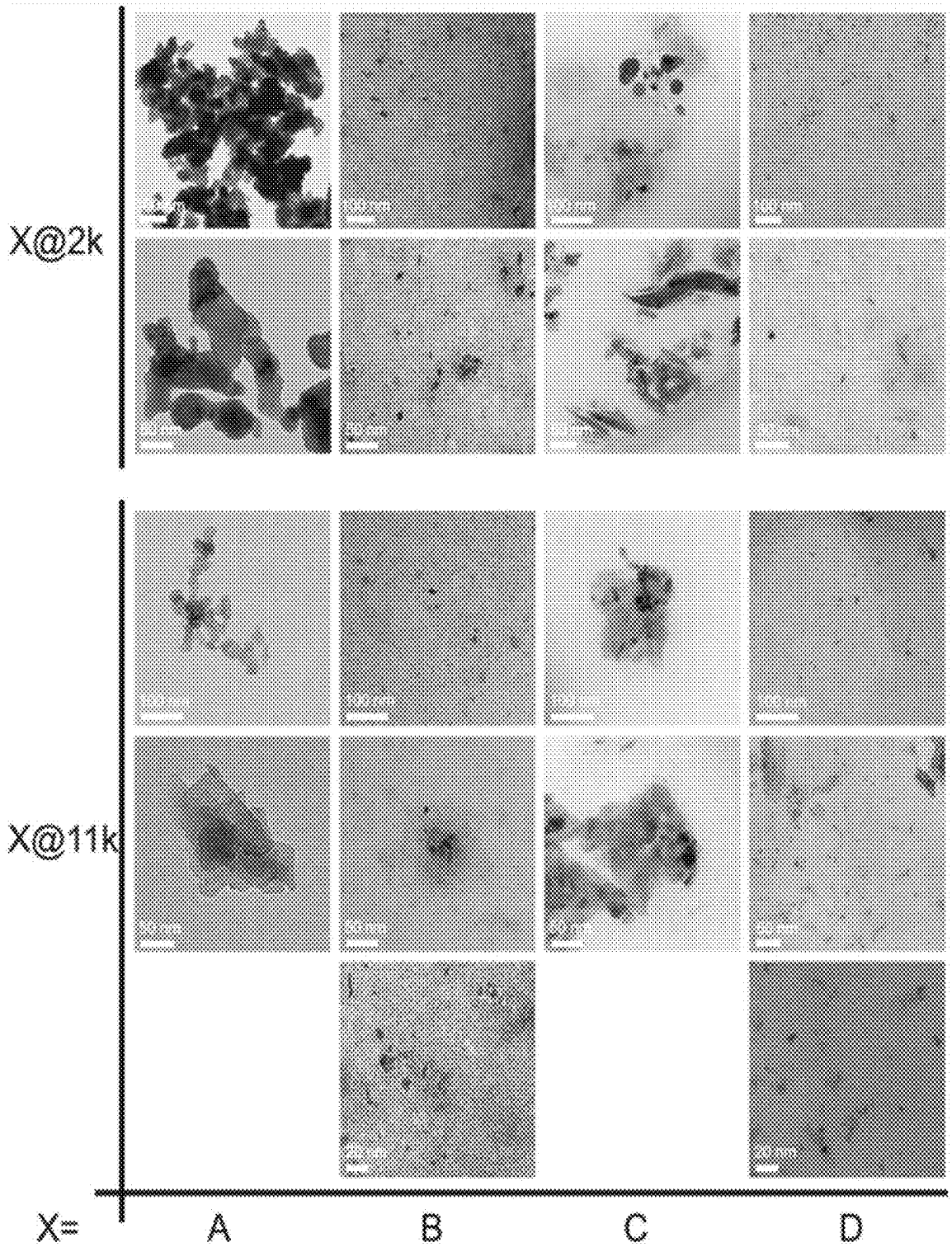

FIG. 6

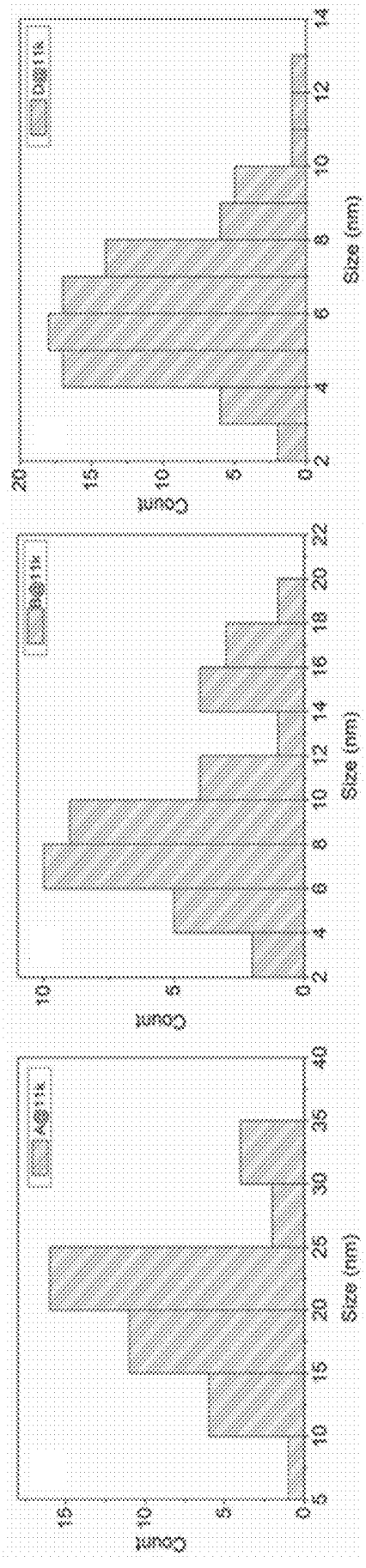

FIG. 7A

FIG. 7B

FIG. 7C

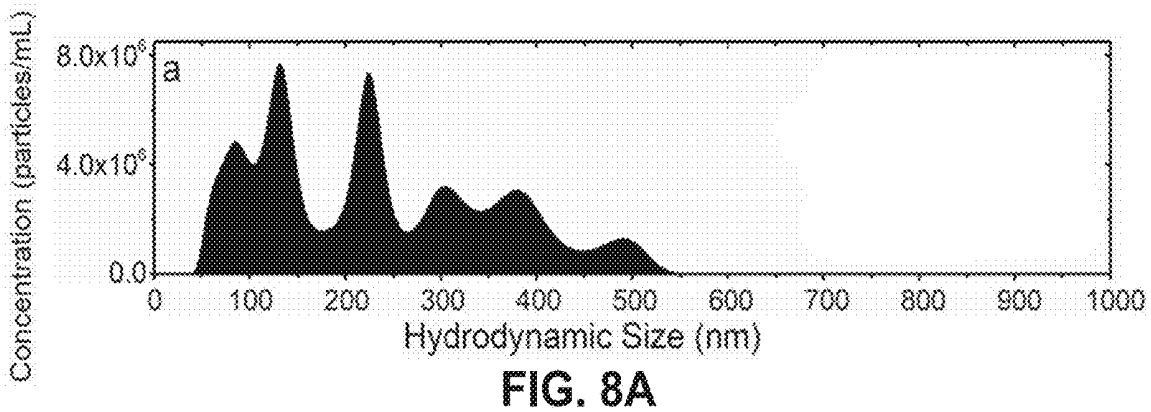

FIG. 8A

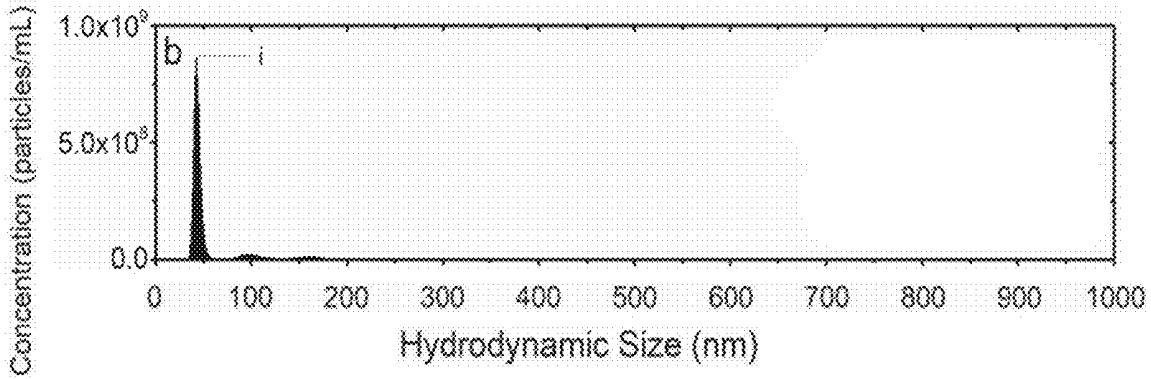

FIG. 8B

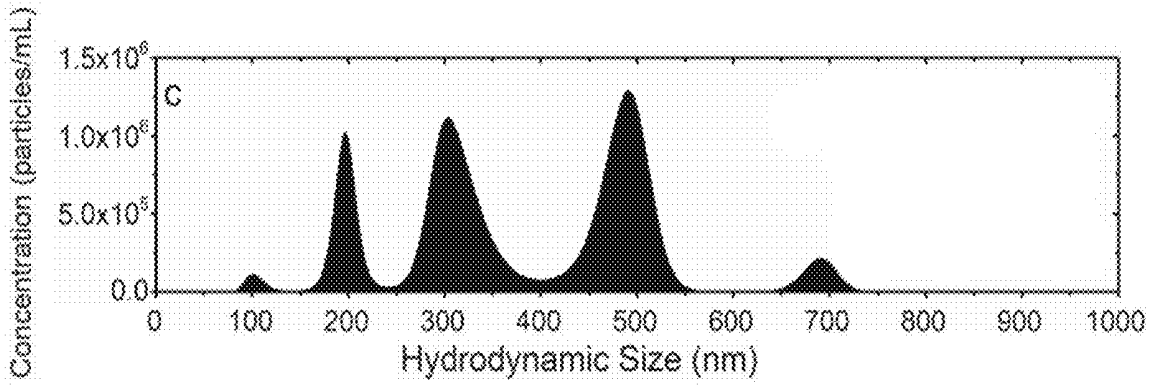

FIG. 8C

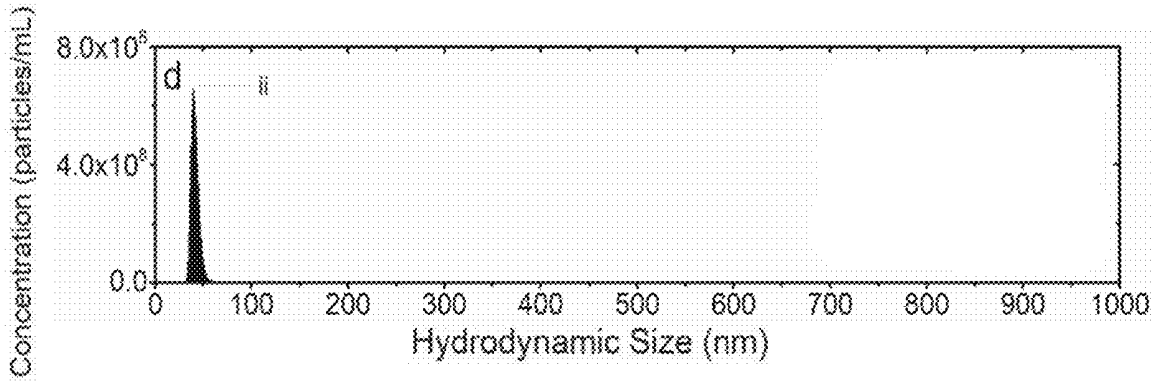

FIG. 8D

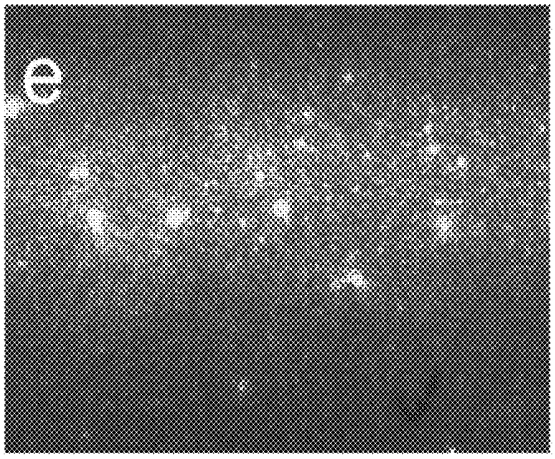

FIG. 8E

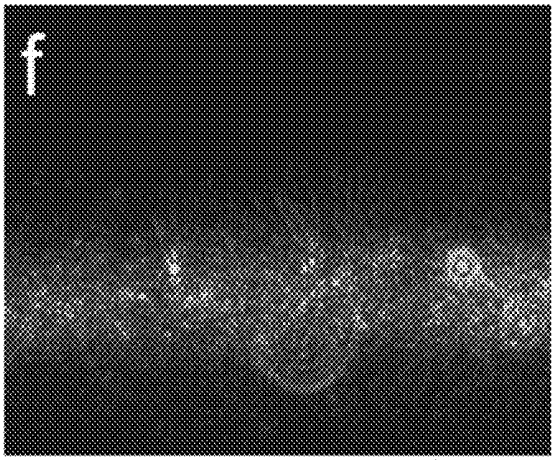

FIG. 8F

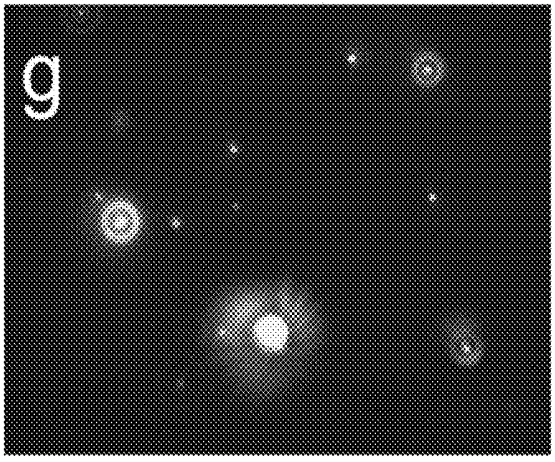

FIG. 8G

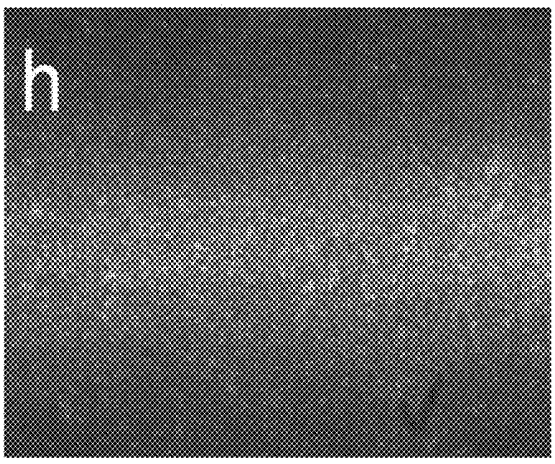

FIG. 8H

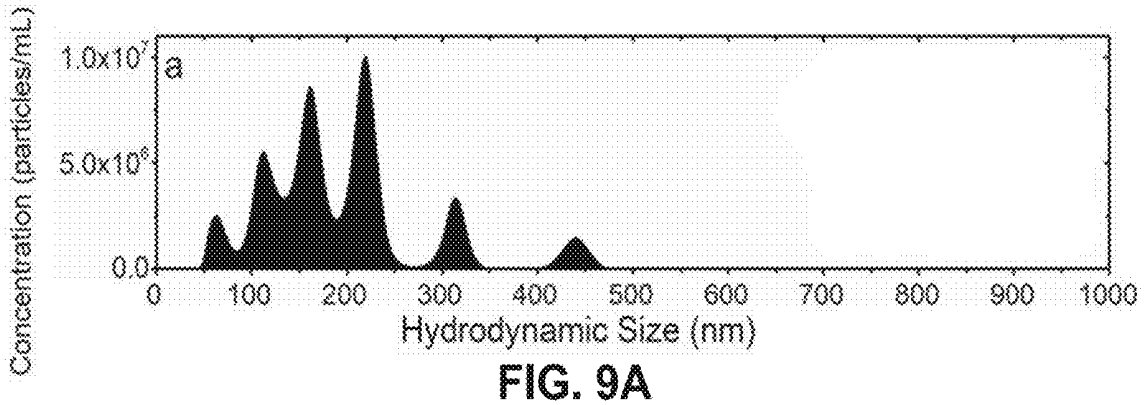

FIG. 9A

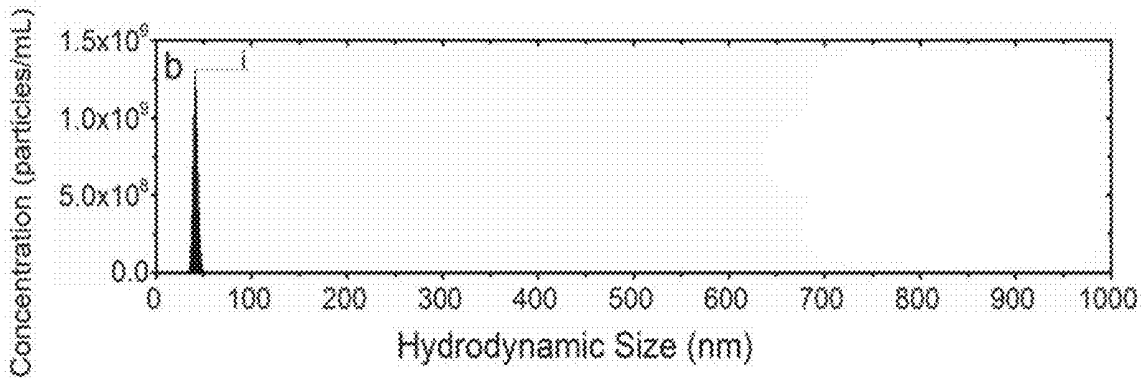

FIG. 9B

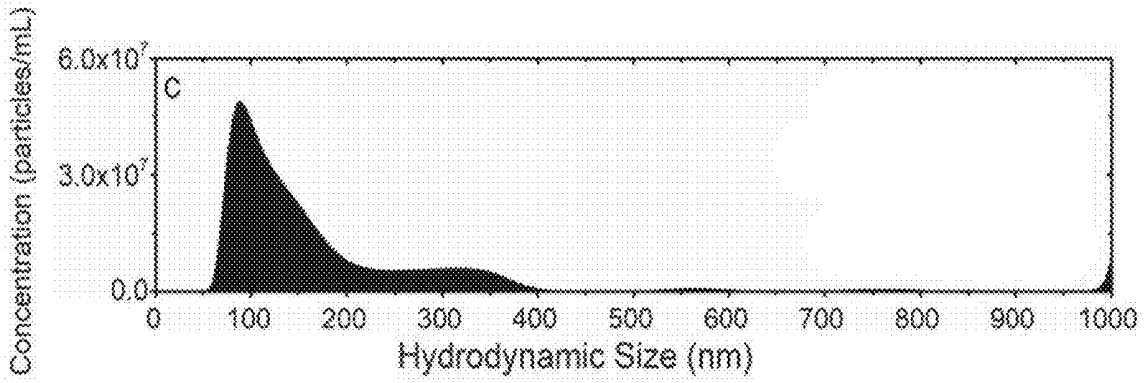

FIG. 9C

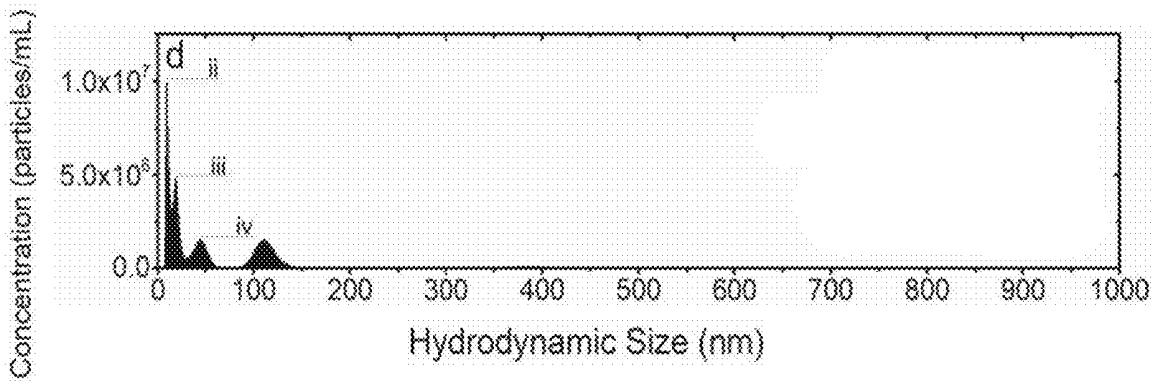

FIG. 9D

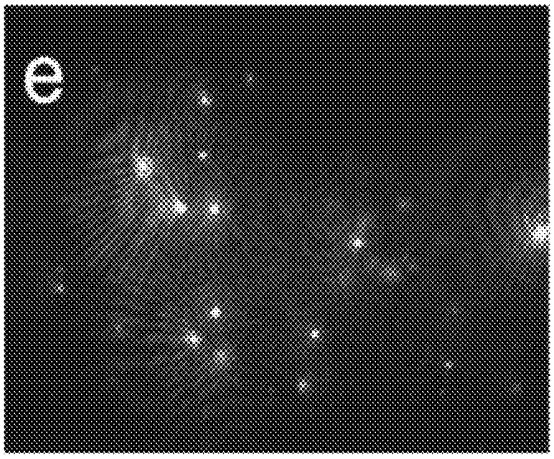

FIG. 9E

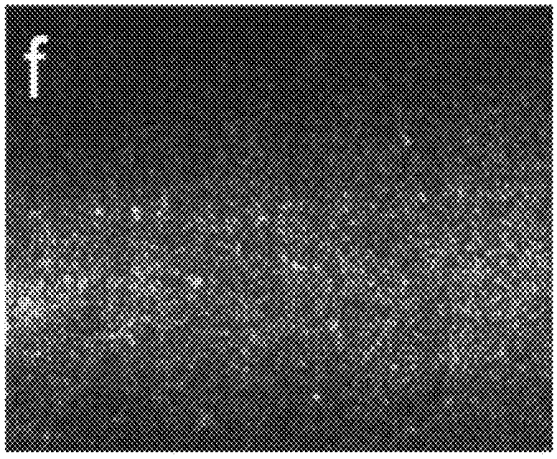

FIG. 9F

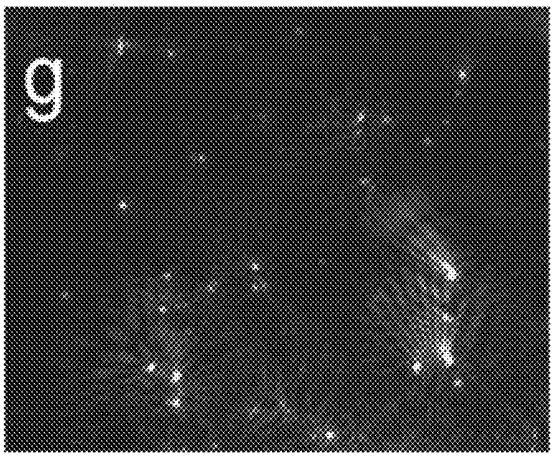

FIG. 9G

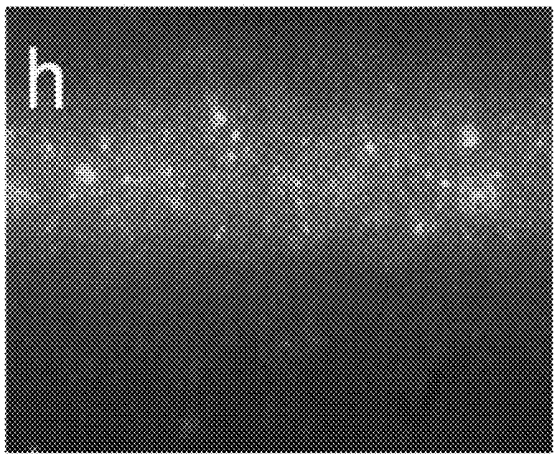

FIG. 9H

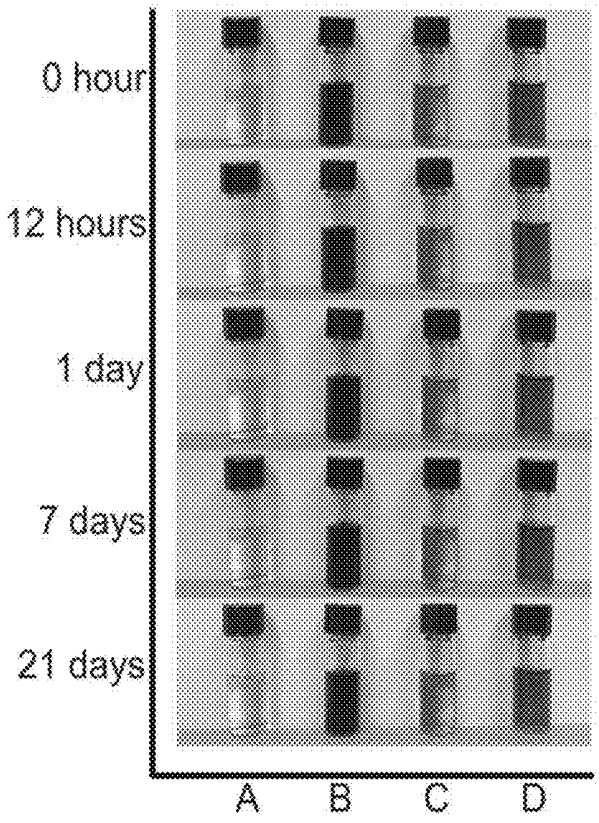

FIG. 10A

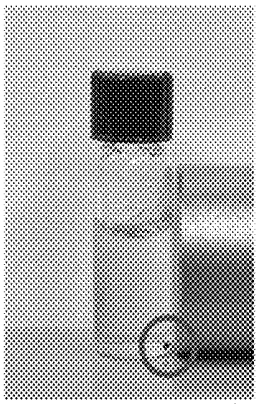

FIG. 10B

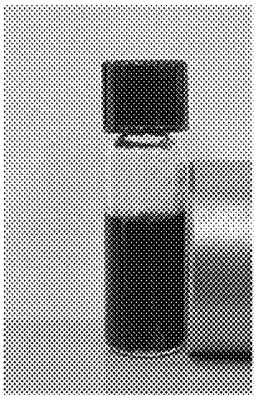

FIG. 10C

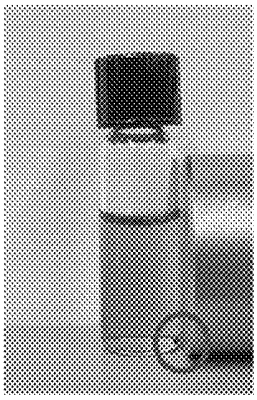

FIG. 10D

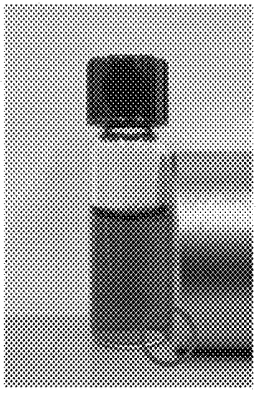

FIG. 10E

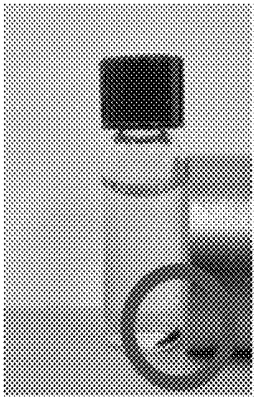

FIG. 10F

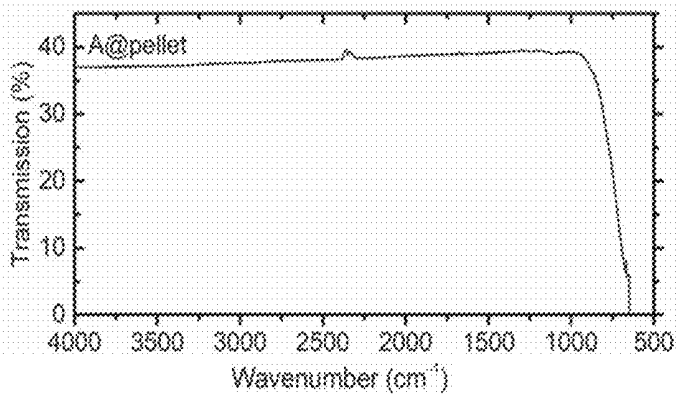

FIG. 11A

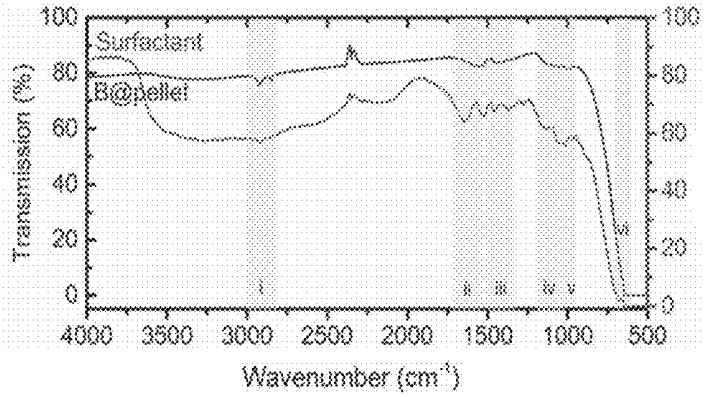

FIG. 11B

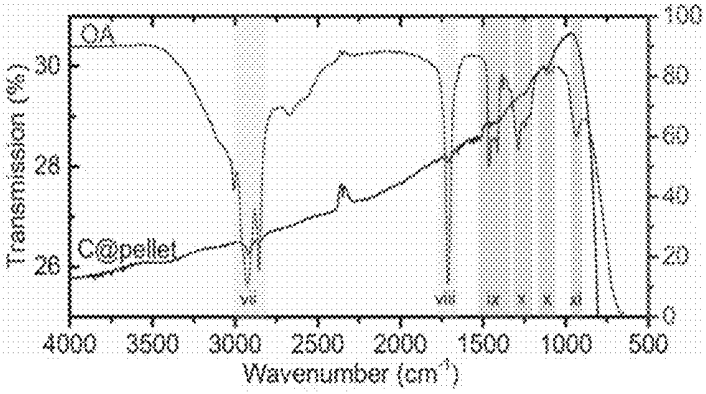

FIG. 11C

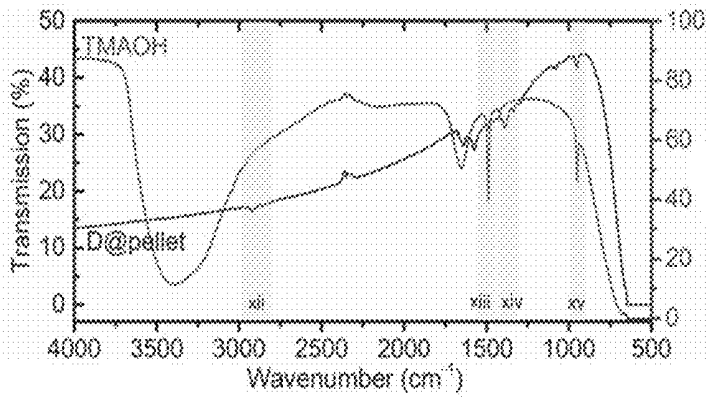

FIG. 11D

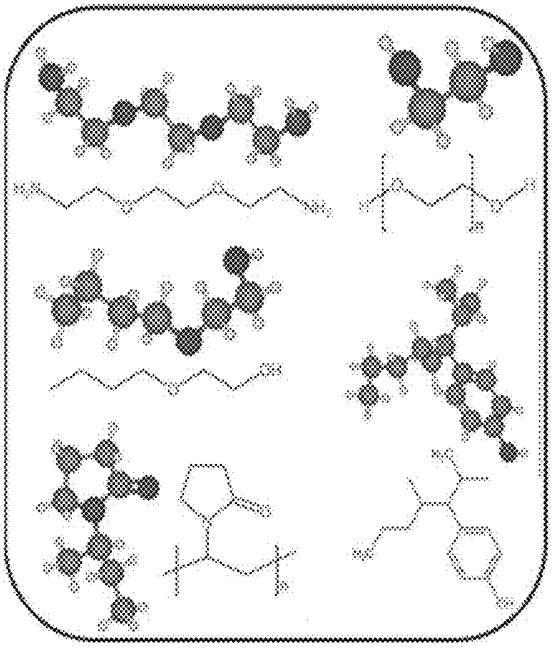

FIG. 11E

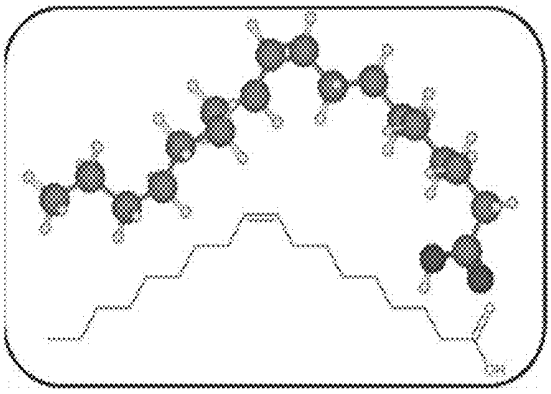

FIG. 11F

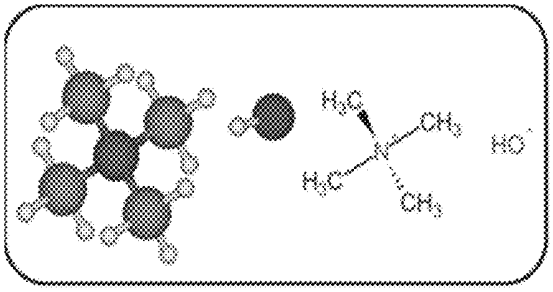

FIG. 11G

FIG. 12A

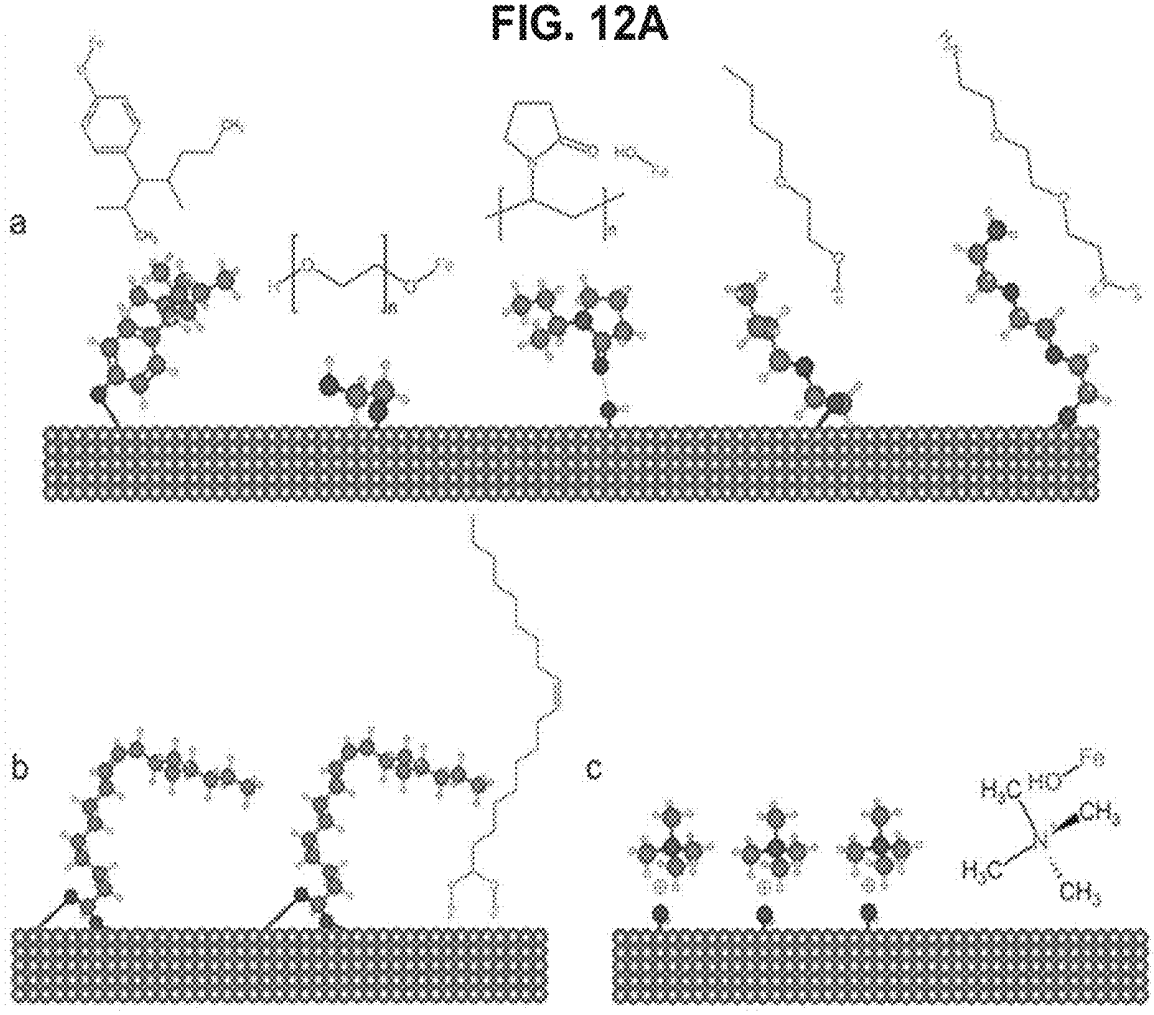

FIG. 12B

FIG. 12C

FIG. 13A

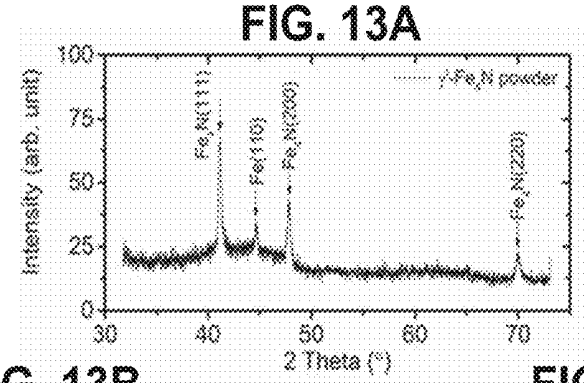

FIG. 13B

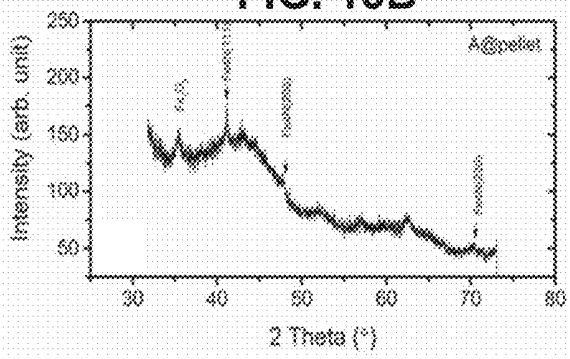

FIG. 13C

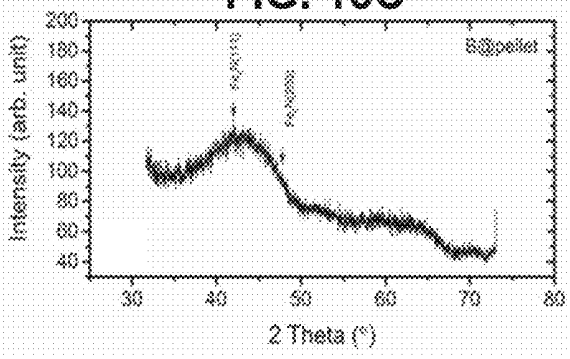

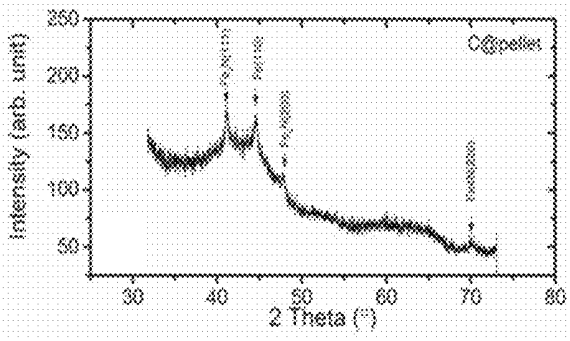

FIG. 13D

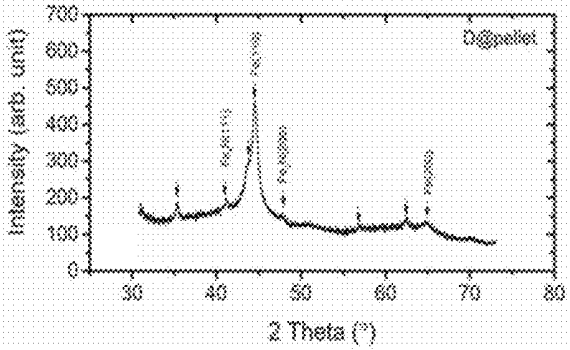

FIG. 13E

IRON NITRIDE NANOPARTICLE SUSPENSION

[0001] This application claims the benefit of U.S. Provisional Patent Application No. 63/201,246, filed Apr. 20, 2021, the entire contents of which is incorporated herein by reference.

TECHNICAL FIELD

[0002] The disclosure relates to magnetic nanoparticles and techniques for forming magnetic nanoparticles.

BACKGROUND

[0003] Iron oxide nanoparticles (IONPs) have been widely used for magnetic diagnosis and treatment such as magnetic resonance imaging (MRI), magnetic particle imaging (MPI), gene/drug delivery, magnetic hyperthermia therapy, magnetic separation, and magnetic biosensors. The research interest in pursuing inexpensive, high magnetic moment, low biotoxicity, colloidal stable, and environmentally friendly magnetic nanoparticles (MNPs) is growing rapidly in view of the increasing demands of high sensitivity magnetic diagnosis and low dose treatments. To this end, γ'-Fe_4N is one promising candidate, because 1) both iron and nitrogen are inexpensive, low biotoxicity, and environment friendly; and 2) the saturation magnetization of γ'-Fe_4N is around two times higher than that of IONPs. Minnealloy α"-$Fe_{16}N_xZ_{2-x}$ or α'-$Fe_8N_xZ_{1-x}$) is another promising candidate, because of its giant saturation magnetization and ultralow magnetic anisotropy constant.

SUMMARY

[0004] In some examples, the disclosure describes a method that includes wet ball milling a plurality of iron nitride nanoparticles in the presence of a surface active agent to modify a surface of the plurality of iron nitride nanoparticles and form a plurality of surface-modified iron nitride nanoparticles.

[0005] In some examples, the disclosure describes a suspension that includes a solvent and a plurality of surface-modified iron nitride nanoparticles suspended in the solvent.

[0006] The details of one or more aspects of the disclosure are set forth in the accompanying drawings and the description below. Other features, objects, and advantages of the techniques described in this disclosure will be apparent from the description, drawings, and claims.

BRIEF DESCRIPTION OF DRAWINGS

[0007] FIG. **1** is a flow diagram illustrating an example technique for forming magnetic nanoparticles that include iron nitride (e.g., γ'-Fe_4N, γ'-$Fe_4N_xZ_{1-x}$, α'-Fe_8N, α"-$Fe_{16}N_xZ_{2-x}$, or α'-$Fe_8N_xZ_{1-x}$, wherein Z comprises at least one of C, B, P, Si, or O).

[0008] FIG. **2**A is a conceptual diagram of an example tube furnace.

[0009] FIG. **2**B is a series of example space-filling models of γ-Fe_2O_3, Fe, and γ'-Fe_4N crystal structure transitions from reduction and nitridation steps.

[0010] FIG. **2**C shows example space-filling models of nitrogen atoms on the surface of an Fe nanoparticle.

[0011] FIGS. **3**A-**3**E show schematic views of example γ'-Fe_4N nanoparticle surface modification steps.

[0012] FIG. **4** illustrates a series of photographs of the samples at various stages of FIGS. **3**A-**3**E.

[0013] FIGS. **5**A and **5**B are static magnetic hysteresis loops of γ-Fe_2O_3 nanoparticles and synthesized γ'-Fe_4N nanoparticles.

[0014] FIG. **5**C shows XRD patterns of γ-Fe_2O_3 nanoparticles and synthesized γ'-Fe_4N nanoparticles.

[0015] FIG. **5**D shows ball-and-stick models of γ-Fe_2O_3, Fe, and γ'-Fe_4N.

[0016] FIG. **6** shows a series of TEM images of X@2k and X@11k samples (X=A, B, C, and D) under different scale bars.

[0017] FIGS. **7**A-**7**C are plots of magnetic core size distributions of γ'-Fe_4N nanoparticles from samples X@11k obtained from the TEM images.

[0018] FIGS. **8**A-**8**D are plots showing the hydrodynamic size distributions of X@2k samples, X=A, B, C, and D, respectively, measured by NTA.

[0019] FIGS. **8**E-**8**H are NTA photos of γ'-Fe_4N nanoparticles from X@2k samples.

[0020] FIGS. **9**A-**9**D are plots showing the hydrodynamic size distributions of X@11k samples, X=A, B, C, and D, respectively, measured by NTA.

[0021] FIGS. **9**E-**9**H are NTA photos of γ'-Fe_4N nanoparticles from X@11k samples.

[0022] FIG. **10**A shows a series of photos of suspensions including surface functionalized γ'-Fe_4N nanoparticles through a 21-day observation period.

[0023] FIGS. **10**B-**10**F show magnetically separated γ'-Fe_4N nanoparticle wet cakes by a permanent magnet.

[0024] FIGS. **11**A-**11**D illustrate IR transmittance spectrums of samples X@pellet.

[0025] FIGS. **11**E-**11**G illustrate the chemical structures of original surface-active media.

[0026] FIGS. **12**A-**12**C show schematic views of chemical groups bonding to Fe atoms through the hydroxyl groups on the surface of γ'-Fe_4N nanoparticles.

[0027] FIGS. **13**A-**13**E illustrate crystal structure characterizations on synthesized γ'-Fe_4N nanoparticle powder and X@pellet samples.

DETAILED DESCRIPTION

[0028] Iron nitride (such as γ'-Fe_4N, α'-Fe_8N, α"-$Fe_{16}N_xZ_{2-x}$, or α'-$Fe_8N_xZ_{1-x}$, wherein Z comprises at least one of C, B, or O) is one promising candidate for a material in magnetic nanoparticles, as 1) both iron and nitrogen are inexpensive, low biotoxicity, and environment friendly, and 2) the saturation magnetization of γ'-Fe_4N is around two times higher than that of IONPs. A comparison of bulk magnetic materials is shown below in Table 1.

TABLE 1

Comparison of Magnetic Properties of Different Bulk Materials

Material	M_s (emu/g)	K (erg/cm^3)	Critical size (diameter) to be superparamagnetic (nm)
Fe_3O_4	98	-1.1×10^5	26
γ-Fe_2O_3	82	-4.6×10^4	35
FeCo	242	10^5	27
Fe	221	$K_1 = 4.8 \times 10^5$ $K_2 = \pm 0.5 \times 10^5$	16
γ'-Fe_4N	184	2.9×10^5	19

TABLE 1-continued

Comparison of Magnetic Properties of Different Bulk Materials

Material	M_s (emu/g)	K (erg/cm^3)	Critical size (diameter) to be superparamagnetic (nm)
α''-$Fe_{16}N_2$	226	9.6×10^6	5.9
α''-$Fe_{16}CN$	258	2.4×10^6	9.4

[0029] In view of saturation magnetizations, iron nitride nanoparticles (γ'-Fe_4N, α'-Fe_8N, α''-$Fe_8N_{2-x}Z_x$ and α'-$Fe_8N_{1-x}Z_x$ nanoparticles, where Z includes at least one of C, B, or O) and FeCo nanoparticles show higher saturation magnetizations over iron oxide. However, FeCo cannot be directly used in biomedical applications because of the concerns of oxidation and corrosion. Thus, using FeCo requires a core-shell structure nanoparticle, with the high saturation FeCo magnetization material as the core and protective biocompatible nonmagnetic materials as the shell to prevent oxidation as well as improve biocompatibility. This reduces the overall saturation magnetization of the core-shell nanoparticles.

[0030] The preparation of colloidally stable, uniformly sized, and sub-100-nm γ'-Fe_4N nanoparticles for biomedical applications is challenging. A gas nitriding method has been used to mass production γ'-Fe_4N nanoparticles. In the gas nitriding method, IONPs may be used as a precursor and a hydrogen reduction step is carried out to remove oxygen and obtain reduced Fe nanoparticles. Next, a mixture of ammonia and hydrogen gas is used to nitride the Fe nanoparticles at a temperature between about 400° C. and about 600° C. Single-phase γ'-Fe_4N nanoparticles have been reported using this method. Although the high temperature gas nitriding approach can realize massive production of high-magnetic-moment γ'-Fe_4N nanoparticles, due to the relatively high processing temperature, some nanoparticles are sintered together, leading to a larger and wider size distribution of the resulting material. The sintered, larger nanoparticles show remanent magnetization (i.e., are not superparamagnetic, showing magnetizations at zero external field). This type of nanoparticles will agglomerate and may block the blood vessels for in vivo applications (such as hyperthermia therapy) and will cause non-uniform magnetic signals for in vitro bioassays. Such material may be less useful, as nanoparticles that are sub-100-nm and with a narrow size distribution are required for most biomedical applications. Further, gas nitriding produces dry γ'-Fe_4N nanoparticles, in which weak forces such as electrostatics, van der Walls forces, and capillary effects may reduce stability of colloidal solutions of the γ'-Fe_4N nanoparticles. Although there have been many reports of the stabilization of IONPs with different functional groups in various solution conditions, direct surface chemical modification of γ'-Fe_4N nanoparticles has not been reported. This disclosure describes example, synthesis and surface functionalization strategies for obtaining stable, substantially monodispersed, sub-100-nm, narrow-size-distributed γ'-Fe_4N nanoparticle colloidal suspensions.

[0031] This disclosure describes synthesis methods for γ'-Fe_4N nanoparticles through a gas nitriding approach. These γ'-Fe_4N nanoparticles are then surface functionalized using wet ball milling and a surface-active media such as a commercially available nanoparticle surfactant, oleic acid (OA), or tetramethylammonium hydroxide solution (TMAOH). The surface-active nanoparticles then may be separated using a centrifugation process to collect the uniformly sized, sub-100-nm γ'-Fe_4N nanoparticles from the supernatants. The morphologies and hydrodynamic sizes of processed γ'-Fe_4N nanoparticles, as well as the surface chemical groups on nanoparticles were characterized by the standard transmission electron microscope (TEM), nanoparticle tracking analyzer (NTA), and Fourier-transform infrared spectroscopy (FTIR). The colloidal stability of processed γ'-Fe_4N nanoparticle suspensions was evaluated by a zeta potential analyzer (ZPA) and through a 21-day period observation period.

[0032] FIG. **1** is a flow diagram illustrating an example technique for forming magnetic nanoparticles that include iron nitride (e.g., γ'-Fe_4N, α'-Fe_8N, α''-$Fe_{16}N_xZ_{2-x}$, or α'-$Fe_8N_xZ_{1-x}$, wherein Z comprises at least one of C, B, or O). The technique of FIG. **1** optionally includes forming a plurality of iron nitride nanoparticles using a gas phase nitriding process (**12**). In some examples, the technique of FIG. **1** may omit step (**12**) and may begin with the following step.

[0033] In examples in which a plurality of iron nitride nanoparticles are formed using a gas phase nitriding process (**12**), the gas phase nitriding process may include placing a plurality of precursor nanoparticles in a furnace. The precursor nanoparticles may include iron oxide (e.g., γ-Fe_2O_3) nanoparticles, iron (e.g., elemental Fe) nanoparticles, or other iron-containing nanoparticles (e.g., iron carbide, iron boride, or the like). The furnace may include any suitable furnace, including a tube furnace.

[0034] In some examples in which the precursor nanoparticles include iron oxide, the gas phase nitriding process may include reducing the plurality of iron oxide nanoparticles to form a plurality of iron nanoparticles. In examples in which the precursor nanoparticles do not include iron oxide (e.g., examples in which the precursor nanoparticles include elemental iron, iron carbide, or iron boride), the reducing step may be omitted. The precursor nanoparticles may be reduced by introducing a reducing gas into the furnace. The reducing gas may include, for example, hydrogen gas, alone or mixed with another gas. In some examples, the reducing step may occur at a temperature of between about 350° C. and about 450° C. and a time between about 2 hours and about 5 hours.

[0035] Once the optional reduction step is complete, the resulting nanoparticles may include iron, iron carbide, iron boride, or the like. The nanoparticles then may be nitride. The nitriding may be performed by exposing the nanoparticles to elemental nitrogen or a nitrogen-containing compound, such as ammonia, urea, diatomic nitrogen, ammonium nitride, an amide, hydrazine, or the like. The nitriding may be performed at a temperature of between about 350° C. and about 450° C. (such as about 400° C.) and a time between about 2 hours and about 3 hours.

[0036] In some examples, during the nitriding step additional elements may be introduced to the nanoparticles. For example, at least one of carbon, boron, phosphorus, silicon, or oxygen may be introduces to the nanoparticles. Such elements may result in the formation of Fe_4N, $Fe_4N_xZ_{1-x}$, α''-$Fe_{16}N_{2-x}Z_x$ and/or α'-$Fe_8N_{1-x}Z_x$, where Z includes at least one of C, B, P, Si, or O. Sources of carbon may include carbon monoxide, carbon dioxide, methane, graphite, urea,

or the like. Some compounds may be used as a source of both carbon and nitrogen, such as urea.

[0037] The nitriding may form nanoparticles including iron nitride. The iron nitride may include at least one of γ'-Fe_4N, γ'-$Fe_4N_xZ_{1-x}$, α'-Fe_8N, α"-$Fe_{16}N_xZ_{2-x}$, or α'-$Fe_8N_xZ_{1-x}$, wherein Z comprises at least one of C, B, P, Si, or O. In some examples, the nanoparticles may include a mixture of iron nitride phases, may include iron nitride and one or more iron phases, or the like.

[0038] Regardless of whether the iron nitride is formed (**12**) or purchase, the technique of FIG. **1** then includes wet ball milling a plurality of iron nitride nanoparticles in the presence of a surface active agent to modify a surface of the plurality of iron nitride nanoparticles and form a plurality of surface-modified iron nitride nanoparticles (**14**). The iron nitride nanoparticles may include any of those described above, including at least one of γ'-Fe_4N, γ'-$Fe_4N_xZ_{1-x}$, α'-Fe_8N, α"-$Fe_{16}N_xZ_{2-x}$, or α'-$Fe_8N_xZ_{1-x}$, wherein Z comprises at least one of C, B, P, Si, or O. The surface-modifying agent may include any agent that reacts with a surface of the iron nitride nanoparticles to form a surface layer on the iron nitride nanoparticles. For example, the surface-modifying agent include at least one hydroxyl group that reacts with a surface of the iron nitride nanoparticles to form a surface layer on the iron nitride nanoparticles. Example surface-modifying agents include sources of at least one of polyvinylpyrrolidone, a polyoxyalkylene amine derivative, polyethylene glycol, ethylene glycol monobutyl ether, nonylphenol, or tetramethylammonium hydroxide.

[0039] The wet ball milling may be performed for between about 1 hour and about 10 hours at an rpm of between about 100 rpm and about 1000 rpm. The wet ball milling may help break up any sintered or agglomerated nanoparticle clumps while the surface modification reaction is proceeding.

[0040] The technique of FIG. **1** then optionally includes centrifuging the plurality of surface-modified iron nitride nanoparticles to separate a set of surface-modified iron nitride nanoparticles having a selected size profile from the plurality of surface-modified iron nitride nanoparticles (**16**). In some examples, the plurality of surface-modified iron nitride nanoparticles may be centrifuged at an rpm and for a time selected to obtain a set of surface-modified iron nitride nanoparticles having an average diameter of less than about 100 nm, or less than about 50 nm. In some implementations, the plurality of surface-modified iron nitride nanoparticles may be centrifuged at an rpm and for a time selected to obtain a set of surface-modified iron nitride nanoparticles having a substantially unimodal size distribution (e.g., at least 90% of the nanoparticles in the set have a size distributed around a single peak). In some examples, centrifuging the plurality of surface-modified iron nitride nanoparticles may be performed at an rpm between about 1,000 rpm and about 50,000 rpm, such as about 2,000 rpm or about 11,000 rpm.

[0041] The technique of FIG. **1** may optionally include further processing the surface-modified iron nitride nanoparticles into one or more mixtures or bulk materials. As one example, the surface-modified iron nitride nanoparticles may be selected for a relatively low average diameter and substantially unimodal size distribution and dispersed into a carrier fluid for use as a biomedical or therapeutic agent. As another example, the surface-modified iron nitride nanoparticles may have a wide distribution of hydrodynamic sizes due to surface functionalization and/or irregular shape, and may be selected to produce a mixture having a corresponding high magnetic field gradient.

[0042] In some examples, the surface-modified iron nitride nanoparticles may be consolidated into a bulk material, such as a soft magnet material. As one example, the surface-modified iron nitride nanoparticles may be dried and compacted into a dense bulk material having grain sizes that correspond to an average diameter of the surface-modified iron nitride nanoparticles. As another example, the surface-modified iron nitride nanoparticles may be dried and dispersed in a binder to form a composite material. The consolidated surface-modified iron nitride nanoparticles may have an irregular shape due to the forces exerted on the iron nitride nanoparticles during wet ball milling, and may be reflected by a high hydrodynamic size, surface area to volume ratio, or other measure of irregularity of a shape or surface.

[0043] Iron nitride nanoparticles produced using the techniques described herein may be used in a variety of applications in which high uniformity, high magnetic saturation, and/or low coercivity may be desired. In some examples, iron nitride nanoparticles may be used in biomedical applications including, but not limited to, magnetic resonance imaging (MRI), magnetic particle imaging (MPI), gene/drug delivery, magnetic hyperthermia therapy, magnetic separation, magnetic biosensors, and the like. As one example, a suspension of iron nitride nanoparticles surface functionalized through wet milling and subsequently centrifuged may have a relatively low size (e.g., an average diameter of less than about 20 nm) and high size uniformity (e.g., a 90% size distribution around a single peak) of the iron nitride nanoparticles. As another example, iron nitride nanoparticles formed by wet milling may have an irregular shape that produces a wide distribution of hydrodynamic sizes, resulting in increased transverse relaxivity. As a result, an MRI contrast agent that includes irregularly shaped iron nitride nanoparticles may have increased contrast.

[0044] In some examples, iron nitride nanoparticles may be used in soft magnet applications including, but not limited to, inductors, transformers, generators, motors, and the like. For example, iron nitride nanoparticles may be processed into a material having a high saturation magnetization (e.g., >180 emu/g) and low coercivity. Iron nitride nanoparticles having a sub-100 nm average diameter may be compacted or composited, alone or with a binder, to form a dense soft magnetic material. This soft magnetic material may have a relatively small grain size (e.g., <100 nm) corresponding to the small average diameter of the iron nitride nanoparticles, resulting in relatively low coercivity. The soft magnetic material may be incorporated into power electronics and other high temperature, high magnetic field devices.

EXAMPLES

[0045] The γ-Fe_2O_3 nanoparticle powder was purchased from MTI Corporation. Commercial nanoparticle surfactant (in water dispersion) was purchased from US Research Nanomaterials, Inc. This surfactant product is a mixture of following substances: Nonylphenol ($C_{15}H_{24}O$, CAS#: 25154-52-3), Polyoxyalkylene amine derivative (CAS#: 68511-96-6), polyethylene glycol ($C_{14}H_{22}O(C_2H_4O)_n$, n=9-10, CAS#: 9002-93-1), Polyvinylpyrrolidone ($((C_6H_9NO)_n$, CAS#: 9003-39-8), Butyl ethanoate ($C_6H_{12}O_2$, CAS#: 123-86-4), Ethylene glycol monobutyl ether ($C_6H_{14}O_2$, CAS#:

111-76-2). Oleic acid ($C_{18}H_{34}O_2$, CAS#: 112-80-1) was purchased from Thermo Fisher Scientific. Tetramethylammonium hydroxide solution ($N(CH_3)_4OH$, CAS#: 75-59-225, wt. % in water) was purchased from Sigma Aldrich.

Synthesis of γ'-Fe_4N Nanoparticles

[0046] γ-Fe_2O_3 nanoparticles (nominal diameter of about 20 nm) were used to prepare γ'-Fe_4N by a gas nitriding approach. The γ-Fe_2O_3 nanoparticles were put in a tube furnace with a diameter of 1 inch, as shown in FIG. **2**A. Once the 100 sccm H_2 gas was introduced, the furnace temperature was increased from room temperature to between about 350° C. and about 450° C. at a rate of about 10° C./min. The γ-Fe_2O_3 nanoparticles were reduced in hydrogen for between about 2 hours and about 5 hours to obtain Fe nanoparticles. This process corresponds to the reduction step labelled in FIG. **2**B. Once the reduction was complete, the temperature of the tube furnace was kept at about 400° C. and ammonia at a rate of 60 sccm (or 40 sccm) and hydrogen at a rate of 20 sccm (or 40 sccm) were introduced into the tube furnace for nitriding as labelled in FIG. **2**B. FIG. **2**B is a series of space-filling models of γ-Fe_2O_3, Fe, and γ'-Fe_4N crystal structure transitions from reduction and nitridation steps.

[0047] The nitriding was performed for between 2 hours and 3 hours. Active nitrogen reacts with the reduced Fe to form γ'-Fe_4N, which is shown in the schematic drawing in FIG. **2**C, which shows space-filling models of nitrogen atoms on the surface of an Fe nanoparticle. As shown in FIG. **2**C, nitrogen atoms diffuse into reduced Fe nanoparticles to form γ'-Fe_4N. The insets shown in FIG. **2**C are the TEM images of Fe and γ'-Fe_4N nanoparticles. After the nitriding was complete, the tube furnace was cooled to 50° C., then the γ'-Fe_4N nanoparticles were directly transferred to a glove box under a nitrogen atmosphere. The samples for vibrating sample magnetometer (VSM) and X-ray diffraction (XRD) were also prepared in the glove box to avoid further oxidation.

γ'-Fe_4N Nanoparticles Surface Modification

[0048] Four γ'-Fe_4N nanoparticle suspensions were prepared through a wet ball milling and centrifugation process. FIGS. **3**A-**3**E show schematic views of γ'-Fe_4N nanoparticle surface modification steps. To begin with, four samples of γ'-Fe_4N nanoparticle powder in surface-active media were prepared. Sample A included 50 mg of γ'-Fe_4N nanoparticle powder was dispersed in 5 mL water. Sample B included 50 mg of γ'-Fe_4N nanoparticle powder dispersed in 5 mL of a 5 vol/vol % commercial nanoparticle surfactant in water. Sample C included 50 mg of γ'-Fe_4N nanoparticle powder dispersed in 5 mL of a 25 vol/vol % oleic acid (OA) in ethanol solution. Sample D included 50 mg of γ'-Fe_4N nanoparticle powder dispersed in 5 mL of a 25 wt. % tetramethylammonium hydroxide (TMAOH) in water solution, as shown in FIG. **3**A. Each sample was then wet ball milled at 350 rpm for 4 hours with time intervals of 30 min, as shown in FIG. **3**B.

[0049] Despite the high yield in the synthesis of γ'-Fe_4N nanoparticles by means of the gas nitriding approach, due the high temperatures in the gas nitriding process, the sintered masses of nanoparticles with large sizes are not favored for biomedical applications. Thus, a centrifugation step was carried out to maintain the sub-100 nm γ'-Fe_4N nanoparticles and discard larger nanoparticles. There is a trade-off between obtaining the uniformly sized, sub-100 nm nanoparticles and reducing the loss rate of raw materials (i.e., the nanoparticle powder after the wet ball milling step). Two centrifugal speeds, 2,000 rpm and 11,000 rpm, were used to determine the effect of centrifugal speeds on yield and particle size distribution. More nanoparticles were retained, and the particle size distribution was wider when sample was centrifuged at 2,000 rpm. On the other hand, centrifugation at 11,000 rpm resulted in a narrower size distribution, but the number of nanoparticles recovered was lower.

[0050] After the wet ball milling process, the turbid suspensions for each sample were allotted into three 1.5 mL vials. The first vial was centrifuged at 2,000 rpm for 30 min, and a 500 μL of supernatant was drawn from the vial. The surface-functionalized γ'-Fe_4N nanoparticles from the supernatant of each sample was separated using a permanent magnet, then washed three times by either water (for nanoparticles from samples A, B, and D) or ethanol (for nanoparticles from sample C). Finally, the surface-functionalized γ'-Fe_4N nanoparticles from the supernatant of each sample were re-dispersed in water or ethanol solvent to the desired volumes for different characterization purposes. These γ'-Fe_4N nanoparticle suspensions were labeled as X@2k (X=A, B, C, and D), as shown in FIG. **3**C.

[0051] Similarly, the second vial of each sample was centrifuged at 11,000 rpm for 30 min, and 500 μL of supernatant was drawn from the vial. After magnetic separation and wash out (as described above), the surface-functionalized γ'-Fe_4N nanoparticles from the supernatant of each sample were re-dispersed in water or ethanol solvent. These γ'-Fe_4N nanoparticle suspensions were labeled as X@11k (X=A, B, C, and D), as shown in FIG. **3**D. The remaining wet cakes from the bottoms of these vials were magnetically separated, washed three times as described above, dried in a N_2 glove box at room temperature, and labeled as X@pellet (X=A, B, C, and D) for further characterizations.

[0052] The third vial of each sample was centrifugated at 2,000 rpm for 30 min, and a 1 mL of supernatant was drawn from the vial. These supernatants were labeled as X@supernatant (X=A, B, C, and D) and sealed in transparent glass bottles for a 21-day colloidal stability observation, as shown in FIG. **3**E. FIG. **4** illustrates a series of photographs of the samples at various stages of FIGS. **3**A-**3**E.

Magnetic Property Characterization

[0053] Nanoparticles samples, γ-Fe_2O_3 and γ'-Fe_4N were stored in a N_2 glove box to avoid oxidation. All the nanoparticle samples for magnetic characterization were prepared in the N_2 glove box. Certain amounts of nanoparticles were weighed and sealed in parafilms to prevent further oxidation after the samples were taken out of the N_2 glove box. Hysteresis loops were measured by a Physical Properties Measurement System (PPMS, Quantum Design Inc.) to obtain the magnetic properties of these nanoparticles such as the saturation (M_s) and coercivity (H_c).

[0054] The static magnetic hysteresis loops of γ-Fe_2O_3 (the precursor) and the synthesized γ'-Fe_4N nanoparticles are shown in FIGS. **5**A and **5**B. As shown in FIG. **5**A, the magnetization of γ-Fe_2O_3 and γ'-Fe_4N nanoparticles saturate at around 2.5 kOe and 7 kOe, respectively. The calculated specific saturation magnetizations (σ_s) of γ-Fe_2O_3 and syn-

thesized γ'-Fe_4N nanoparticles at 15 kOe are about 57.7 and 182.7 emu/g, respectively. FIG. **5**B is an enlarged view of the hysteresis loops within a magnetic field of ±2 kOe. The coercivities (H_c) of γ-Fe_2O_3 and synthesized γ'-Fe_4N nanoparticles are 0 and 310 Oe, respectively. Since some γ'-Fe_4N nanoparticles were sintered during the high temperature gas nitriding process, these sintered nanoparticles are larger in size thus, unlikely to be superparamagnetic. As a result, the synthesized γ'-Fe_4N nanoparticles show ferromagnetic properties with large magnetic coercivity and remanence as seen in FIG. **3**A. On the other hand, the γ-Fe_2O_3 (the precursor) shows superparamagnetic properties with zero magnetic coercivity and remanence. The specific magnetizations (σ) of both nanoparticles under different magnetic fields, coercivities (H_c), remanence magnetizations (M_r), and magnetic susceptibilities (χ) are summarized in Table 2.

TABLE 2

Magnetic properties comparisons on γ-Fe_2O_3 and the synthesized γ'-Fe_4N nanoparticles.

	M_s (15 kOe)	M (5 kOe)	M (1 kOe)	H_c	M_r	χ (±1 kOe)
γ-Fe_2O_3	57.7 emu/g	51.3 emu/g	38.0 emu/g	0 Oe	0 emu/g	0.038 emu/g/Oe
γ'-Fe_4N	182.7 emu/g	168.0 emu/g	106.3 emu/g	310 Oe	45 emu/g	0.093 emu/g/Oe

[0055] The high H_c and large remanence of γ'-Fe_4N are caused by the sintering during the high temperature gas nitriding process. These sintered γ'-Fe_4N particles with wider size distributions and larger sizes (as shown below in FIG. **6** and FIG. **7**A) are not suitable for most biomedical applications. Thus, a goal of this disclosure is to break these larger sintered particles, separate smaller nanoparticles by a wet ball milling method with surface-active media, then centrifuge to extract and purify monodispersed, uniformly sized, and sub-100-nm γ'-Fe_4N nanoparticles.

Crystal Structure Characterization

[0056] γ-Fe_2O_3 and γ'-Fe_4N nanoparticle samples for X-ray diffraction (XRD) patterns were also prepared in the N_2 glove box. Selected amounts of nanoparticles were put on a piece of glass substrate and an epoxy was used to seal the nanoparticles to prevent oxidation after the samples were taken out of the glove box. When the epoxy dried and solidified, these samples were used to for the XRD measurements. The XRD patterns were characterized using a Bruker D8 Discover 2D equipped with a Co radiation source operated at 45 kV and 40 mA. For a convenient comparison, the XRD patterns were converted into a Cu radiation source using MDI Jade software.

[0057] The XRD patterns of the precursor γ-Fe_2O_3 and synthesized γ'-Fe_4N nanoparticles are shown in FIG. **5**C. The powder diffraction files (PDFs) of these two materials are also plotted at the bottom panels of the XRD patterns. The XRD pattern of starting γ-Fe_2O_3 nanoparticles matches well with the PDF, indicating that the starting materials are γ-Fe_2O_3. These iron oxide nanoparticles are then reduced by hydrogen gas to get rid of oxygen and create preferable microstructures for the following nitriding process. After the nitriding, the XRD patterns show that the main phase is γ'-Fe_4N. Thus, γ'-Fe_4N nanoparticles are successfully synthesized by the gas nitriding approach. Ball-and-stick models of γ-Fe_2O_3 and γ'-Fe_4N are shown in FIG. **5**D to provide a brief view how the crystal structure changes from the γ-Fe_2O_3 to reduced Fe and synthesized γ'-Fe_4N.

Nanoparticle Morphology and Size Characterization

[0058] The morphologies of γ'-Fe_4N nanoparticle cores were characterized by a transmission electron microscope (TEM, FEI Tecnai T12). Briefly, 10 μL of X@2k and X@11k (X=A, B, C, and D) nanoparticle colloidal suspensions were dropped on TEM grids and air dried at room temperature before TEM imaging.

[0059] The hydrodynamic sizes of these surface functionalized γ'-Fe_4N nanoparticles were measured using a nanoparticle tracking analyzer (NTA, Nanosight LM-10). 1.5 mL of samples X@2k and X@11k (X=A, B, C and D) were used for the hydrodynamic size measurements on the NTA. The NTA used a 400 nm (near UV) laser to track the motion of γ'-Fe_4N nanoparticles suspended in solvents (i.e., water for samples A, B, D and ethanol for sample C) then calculated the size distributions for nanoparticles between 10 nm and 1 μm.

[0060] Initially, it should be noted that the TEM morphology imaging was used to observe the magnetic cores of synthesized γ'-Fe_4N nanoparticles, thus, the sizes read from TEM images are different from the hydrodynamic sizes read from NTA.

[0061] FIG. **6** shows a series of TEM images of X@2k and X@11k samples (X=A, B, C, and D) under different scale bars. Samples A and C show severe aggregations of γ'-Fe_4N nanoparticles, while samples B and D show monodispersed nanoparticles even after the centrifugation at 2,000 rpm for 30 min.

[0062] It can be clearly seen that γ'-Fe_4N nanoparticles that are wet ball milled in water (samples A@2k and A@11k) and in oleic acid (OA) (samples C@2k and C@11k) are forming large clusters. This indicates that: 1) wet ball milling in water and OA cannot effectively separate γ'-Fe_4N nanoparticles; 2) these γ'-Fe_4N nanoparticles are not superparamagnetic and thus, forming clusters due to non-zero remanence; and 3) these γ'-Fe_4N nanoparticles processed with water and OA will not be colloidally stable and may form sediments in solvents.

[0063] On the other hand, the γ'-Fe_4N nanoparticles that are wet ball milled in commercial surfactant product and TMAOH are monodispersed. Samples B@2k, B@11k, D@2k, and D@11k show monodispersed and small size γ'-Fe_4N nanoparticles. This indicates that 1) centrifuging at 2,000 rpm for 30 min is sufficient to extract uniform-sized, monodispersed, and sub-100-nm γ'-Fe_4N nanoparticles; and 2) these nanoparticles are not forming clusters and will be colloidally stable. Furthermore, many γ'-Fe_4N nanoparticles

with sizes below 20 nm are observed, while the theoretical size limit for γ'-Fe_4N nanoparticles to be superparamagnetic is 19 nm.

[0064] The magnetic core size distributions of γ'-Fe_4N nanoparticles from samples X@11k were obtained from the TEM images and plotted in FIGS. **7**A-**7**C. Note that sample C@11k shows severe nanoparticle aggregations, and the size distribution was not clear from TEM images. The anisotropy constant of γ'-Fe_4N is reported to be $K_c=2.9\times10^5$ erg/cm^3, and the theoretical critical size is calculated to be 19 nm for γ'-Fe_4N nanoparticles to be superparamagnetic at room temperature. Since water and oleic acid (OA) cannot effectively separate and surface functionalization γ'-Fe_4N nanoparticles, these nanoparticles are likely to cluster. As shown in FIG. **7**A, a wide size distribution from 5 nm to 35 nm was obtained from TEM images for the sample ball milled in water. On the other hand, the sizes of γ'-Fe_4N nanoparticles from samples B@11k and D@11k were below 20 nm, as shown in FIGS. **7**B and **7**C. Thus, superparamagnetic γ'-Fe_4N nanoparticles were obtained from wet ball milling with commercial nanoparticle surfactants and TMAOH and centrifugation steps.

[0065] The NTA was used to measure the hydrodynamic size of the γ'-Fe_4N nanoparticles after different surface modification processes. FIGS. **8**A-**8**D are plots showing the hydrodynamic size distributions of X@2k samples, X=A, B, C, and D, respectively, measured by NTA. FIGS. **8**E-**8**H are the NTA photos of γ'-Fe_4N nanoparticles. (i) and (ii) denote the peaks at 44 nm and 41 nm, respectively. A statistical average of 5 independent NTA measurements was carried out on samples X@2k (X=A, B, C, and D). During each NTA measurement, a 1 min video of the γ'-Fe_4N nanoparticles is recorded under the microscope, and snapshots of the respective samples are given in FIGS. **8**E-**8**H. From FIGS. **8**A & **8**E and FIGS. **8**C & **8**G, it is evident that the γ'-Fe_4N nanoparticles from samples A@2k and C@2k are severely clustered, with prominent peaks at the greater side of the hydrodynamic size. The significant clustering of the nanoparticles is also seen from the TEM images in FIG. **6** for samples A@2k and C@2k. However, from FIGS. **8**B & **8**F and FIGS. **8**D & **8**H, it is evident that the samples B@2k and D@2k show prominent peaks at hydrodynamic sizes of 44 nm and 41 nm, respectively. This is also supported by the TEM images in FIG. **6**. The scale bars in TEM images of FIG. **6** show that some particles are of the order of 20 nm in size, whereas the hydrodynamic size measurements show that sample B@2k mostly has size of 44 nm and sample D@2k mostly has size of 41 nm because the surfactant coatings of nanoparticles sum up to the hydrodynamic size. On the contrary, TEM only captures the core size of the nanoparticles. Table 3 shows the 10^{th}, 50^{th} and 90^{th} percentile as well as the mean hydrodynamic sizes of γ'-Fe_4N nanoparticles from samples X@2k (X=A, B, C and D) as obtained from the NTA measurements.

TABLE 3

Percentile and average sizes of γ'-Fe_4N nanoparticles in X@2k samples (X = A, B, C, and D).

X@2k	A	B	C	D
10^{th}	86.8 nm	39.7 nm	198.1 nm	37.8 nm
50^{th}	220.8 nm	44.4 nm	352.3 nm	41.5 nm
90^{th}	405.3 nm	102.8 nm	514.7 nm	49.8 nm
Average size	233.8 nm	58.5 nm	382.1 nm	45.3 nm

[0066] The hydrodynamic size distributions and percentile size distributions of samples X@11k (X=A, B, C, and D) are provided in FIGS. **9**A-**9**H and Table 4.

[0067] From FIG. **9**A in corroboration with snapshot in FIG. **9**E and FIG. **9**C in corroboration with snapshot in FIG. **9**G, it is evident that the γ'-Fe_4N nanoparticles from samples A@11k and C@11k are severely clustering, with prominent peaks at the greater side of the hydrodynamic size. However, from FIG. **9**B in corroboration with snapshot in FIG. **9**F and FIG. **9**D in corroboration with snapshot in FIG. **9**H, it is evident that the sample B@11k shows prominent peak at 42 nm and sample D@11k shows prominent peaks at 11 nm, 20 nm, and 44 nm, respectively. Due to the ultra-high centrifugal speed, smaller nanoparticles are retained in the supernatants. Thus, 11 nm and 20 nm nanoparticles are dominating in sample D@11k. Table 3 shows the 10^{th}, 50^{th} and 90^{th} percentiles as well as the mean hydrodynamic sizes of nanoparticles from samples X@11k (X=A, B, C and D) as obtained from the NTA measurements.

Colloidal Stability of γ'-Fe_4N Nanoparticles

[0068] The colloidal stabilities of surface functionalized γ'-Fe_4N nanoparticles by different surface-active media were appraised through a 21-day observation period on samples X@supernatant (X=A, B, C, and D). As shown in FIG. **10**A, no observable sedimentations are present in any of these samples. However, this type of observation by bare eyes are not very reliable due to the low amount of γ'-Fe_4N nanoparticles presenting in the suspensions. FIGS. **10**B-**10**F show the magnetically separated γ'-Fe_4N nanoparticle wet cakes by a permanent magnet, proving that there is a small number of nanoparticles in each X@supernatant sample. It should be noted that due to the dark background color of solvent in sample B@supernatant, a second photo of the separated nanoparticles (wet cake) is given in FIG. **10**F after three times of magnetic wash out with water.

Zeta Potential of Nanoparticles

[0069] A zeta potential analyzer (ZPA, Stabino) was used to measure the particle charge distribution or the zeta potential of the surface functionalized γ'-Fe_4N nanoparticles from solvents (water or ethanol). 5 mL of samples X@2k (X=A, B, C, and D) are prepared, sonicated for 30 min before the zeta potential measurements.

[0070] The zeta potentials of surface functionalized γ'-Fe_4N nanoparticles in solvent are −29.13 mV, −26.27 mV, −0.55 mV, and −29.99 mV, respectively for A, B, C, and D. This indicates that γ'-Fe_4N nanoparticles processed by commercial surfactants, water, and TMAOH are relatively stable due to a large electrokinetic potential (or electrostatic repulsion), while, on the other hand, γ'-Fe_4N nanoparticles treated by OA will rapidly coagulate.

[0071] Although zeta potential results indicate γ'-Fe_4N nanoparticles treated by commercial surfactants, water, and

TMAOH should be colloidally stable and that γ'-Fe_4N nanoparticles treated by OA should not be colloidally stable, the TEM images and NTA results show that only the γ'-Fe_4N nanoparticles that are treated by commercial surfactants and TMAOH are uniformly sized and monodispersed, while nanoparticles treated by water are not. This is because, although γ'-Fe_4N nanoparticles treated by water show a large electrokinetic potential (or electrostatic repulsion), there is no surface chemical groups functionalized on these nanoparticles, and the non-zero remanences of these nanoparticles cause clustering.

Nanoparticle Surface Chemical Groups Characterization

[0072] The chemical groups functionalized on γ'-Fe_4N nanoparticle surfaces were characterized by a FTIR spectrometer (Fourier-transform infrared spectroscopy, Thermo Scientific Nicolet iS50 FTIR) on the main detector MCT-A (7000-600 cm^{-1}), with KBr beam splitter and a resolution of 2 cm^{-1}. A total of 32 scans were taken on each sample. Samples X@pellet (X=A, B, C, and D) were evenly spread and dried on a barium fluoride (BaF_2) window (diameter 25.4 mm, thickness 2 mm, purchased from EKSMA Optics, UAB) for FTIR transmittance spectrum collection. In addition, the FTIR transmittance spectrum of the commercial surfactant product, OA, and TMAOH are also collected for direct comparisons. These liquid samples were sealed between two BaF_2 windows before FTIR characterizations.

[0073] The IR transmittance spectrums are given in FIGS. **11**A-**11**D. For comparison, the transmittance spectrums of original surface-active media (commercial surfactant for sample B, OA for sample C, TMAOH for sample D) are plotted in parallel. The grey regions indicate that the characteristic transmittance peaks are observed from both X@pellet and its original surface-active media. The ix, x, x, and xi regions in FIG. **11**C indicate that the characteristic transmittance peaks from original surface-active media are absent from C@pellet sample. The chemical structures of original surface-active media are drawn in parallel with IT transmittance spectrums in FIGS. **11**E-**11**G.

[0074] The FTIR transmittance spectrum of A@pellet in FIG. **11**A does not show any remarkable peaks, thus, γ'-Fe_4N nanoparticles are not functionalized with any chemical groups through wet ball milling process in water. Note that, once the γ'-Fe_4N nanoparticles were brought out of the vacuum chamber, a mixed mode layer of hydroxyl group and water formed on the nanoparticle surface. This caused some weak spikes around 3600 cm^{-1} and 1600 cm^{-1}. Usually, these peaks from water are removed by dehumidifying or pumping the FTIR chamber, subtracted as background spectrum (without sample loaded, only BaF_2 window loaded), and averaged by carrying out 32 FTIR scans. However, from sample C@pellet, as shown in FIG. **11**C, some visible peaks caused by this mixed mode layer of hydroxyl group and water are still present. It does not affect the analysis of FTIR results. On the other hand, this mixed mode layer of hydroxyl group and water facilitates the subsequent nanoparticle surface modifications. FIGS. **12**A-**12**C show schematic views of these chemical groups bonding to the Fe atoms through the hydroxyl groups on the surface of γ'-Fe_4N nanoparticles. The hydroxyl group on the surface of the nanoparticles tend to bond with the chemical groups with high electron affinity. The grain size, chemical structures of the final product can be engineered by optimizing the type and concentration of the surfactants.

[0075] In FIG. **11**B, the chemical groups such as benzene derivative (~700 cm^{-1}, marked as vi in FIG. **11**B) and C═C bending (960-1000 cm^{-1}, marked as v in FIG. **11**B) are from nonylphenol, C—N and C—O stretching (1000-1300 cm^{-1}, marked as vi in FIG. **11**B) come from nonylphenol, polyoxyalkelene amine derivative, polyethylene glycol, polyvinylpyrrolidone, and ethylene glycol monobutyl ether. Other chemical groups and corresponding FTIR transmittance peaks are listed in Table 4. FTIF confirms that the surface-active groups from this commercial surfactant product are successfully functionalized on γ'-Fe_4N nanoparticles after the wet ball milling process. FIG. **12**A gives the schematic views of these chemicals bond on γ'-Fe_4N nanoparticle surface through hydroxyl groups.

TABLE 4

Chemical groups coated on γ'-Fe_4N nanoparticles

Sample index	Label	Chemical group	Sources
B@pellet	i	C—H stretching	All*
		C═O stretching	Polyvinylpyrrolidone
	ii	C—O stretching	Polyoxyalkylene amine derivative, Polyethylene glycol, Ethylene glycol monobutyl ether
		N—H bending	Polyoxyalkylene amine derivative
	iii	O—H bending	Nonylphenol, Polyethylene glycol, Ethylene glycol monobutyl ether
		C—H bending	All*
	iv	C—N stretching	Polyoxyalkylene amine derivative, Polyvinylpyrrolidone
		C—O stretching	Polyoxyalkylene amine derivative, Polyethylene glycol, Ethylene glycol monobutyl ether
	v	C═C bending	Nonylphenol
	vi	Benzene derivative	Nonylphenol
C@pellet	vii	C—H stretching	Oleic acid (OA)
	viii	C═O stretching	
	ix	C—H bending	
	x	C—O stretching	
	xi	C═C bending	
D@pellet	xii	C—H stretching	Tetramethylammonium hydroxide (TMAOH)
	xiii	C—H bending	
	xiv	C—N stretching	
	xv	C—H bending	

*Nonylphenol, Polyoxyalkylene amine derivative, Polyethylene glycol, Polyvinylpyrrolidone, Ethylene glycol monobutyl ether

[0076] The transmittance spectrum of C@pellet is shown in FIG. **11**C. The very weak peaks of C—H stretching (2800-3000 cm^{-1}, marked as vii in FIG. **11**C) and C═O stretching (~1750 cm^{-1}, marked as viii in FIG. **11**C) were observed. However, the stronger C—H bending (1400-1500 cm^{-1}, marked as ix in FIG. **11**C), C—O stretching (~1250 cm^{-1} and 1100 cm^{-1}, marked as x in FIG. **11**C), C═C bending peak at 885-995 cm^{-1}, marked as xi in FIG. **11**C) are absent from C@pellet. Thus, the OA is not successfully functionalized on γ'-Fe_4N nanoparticles. That also explains why these nanoparticles are clustering from TEM images (as shown in FIG. **6**), showing wide and large size distributions (as shown in FIG. **7**C), as well as low zeta potentials. Although the OA groups have been reported to be successfully coated on iron oxide nanoparticle by many groups, unfortunately, only very few amount of OA groups are bond on γ'-Fe_4N nanoparticles. FIG. **12**B shows the schematic views of OA bond on γ'-Fe_4N nanoparticle surface.

[0077] The transmittance spectrum of D@pellet is shown in FIG. **11**D. The characteristic C—H bending and stretch-

ing peaks at 2840-3000 cm^{-1} (marked as xii in FIG. **11**D), 1380-1450 cm^{-1} (marked as xiii in FIG. **11**D), and 880 cm^{-1} (marked as xv in FIG. **11**D), C—N stretching at 1300 cm^{-1} (marked as xiv in FIG. **11**D) are observed. This indicates that TMAOH has been successfully functionalized on γ'-Fe_4N nanoparticles. FIG. **12**C shows the schematic views of TMAOH bond on γ'-Fe_4N nanoparticle surface.

Crystal Structure of Surface Functionalized γ'-Fe_4N Nanoparticles

[0078] During the wet ball milling process, different surfactants were added, and the milling speed was low (350 rpm). The decomposition temperature of γ'-Fe_4N is above 600° C. based on the Fe—N phase diagram. The surfactants, except water, can also help protect nanoparticles from oxidation during the milling process. Thus, the produced nanoparticles should still conserve the original phase and have the similar magnetic properties. To demonstrate that the nanoparticles after wet ball milling with the four surface-active media (A: water, B: 5 vol/vol % commercial nanoparticle surfactant in water, C: 25 vol/vol % OA in ethanol, D: 25 wt % TMAOH in water) are still γ'-Fe_4N, a new batch of γ'-Fe_4N nanoparticles were synthesized and X@pellet samples (X=A, B, C, and D) were prepared as described above. The crystal structure characterizations on the newly synthesized γ'-Fe_4N nanoparticle powder and X@pellet samples are shown in FIGS. **13**A-**13**E. The XRD patterns of newly synthesized γ'-Fe_4N nanoparticles and the γ'-Fe_4N peaks are labeled. However, for this batch of sample, reduced Fe phase is seen due to insufficient nitriding step from FIG. **13**A. But this does not affect the assessment of whether wet ball milling with the four surface-active media will change the crystal structure of nanoparticles. FIGS. **13**B-**13**E shows the XRD patterns of A@pellet, B@pellet, C@pellet, and D@pellet after the wet ball milling process. All the visible Fe_4N (111) and Fe_4N(200) peaks are labeled, as well as the Fe(110) peak (due to insufficient nitriding step, which is shown in the starting material γ'-Fe_4N powder). These figures indicate that the wet ball milling step with four surface-active media does not change the crystal structures of the produced nanoparticles. The crystal structure characterizations by XRD are strong evidence that the produced nanoparticles after ball milling step are still γ'-Fe_4N.

Example 1

[0079] A method includes wet ball milling a plurality of iron nitride nanoparticles in the presence of a surface active agent to modify a surface of the plurality of iron nitride nanoparticles and form a plurality of surface-modified iron nitride nanoparticles.

Example 2

[0080] The method of example 1, wherein the plurality of iron nitride nanoparticles comprise at least one of γ'-Fe_4N, α'-Fe_8N, α"-$Fe_{16}N_xZ_{2-x}$, or α'-$Fe_8N_xZ_{1-x}$, wherein Z comprises at least one of C, B, P, Si, or O.

Example 3

[0081] The method of any of examples 1 and 2, further includes centrifuging the plurality of surface-modified iron nitride nanoparticles to separate a set of surface-modified iron nitride nanoparticles having a selected size profile from the plurality of surface-modified iron nitride nanoparticles.

Example 4

[0082] The method of any of examples 1 through 3, further includes forming the plurality of iron nitride nanoparticles from a plurality of iron oxide nanoparticles using a gas phase nitriding process.

Example 5

[0083] The method of example 4, wherein the plurality of iron oxide nanoparticles comprise a plurality of γ-Fe_2O_3 nanoparticles.

Example 6

[0084] The method of any of examples 4 and 5, wherein the gas phase nitriding process comprises: reducing, in a furnace, the plurality of iron oxide nanoparticles to form a plurality of iron nanoparticles; and nitriding the plurality of iron particles to form the plurality of iron nitride nanoparticles.

Example 7

[0085] The method of example 6, wherein nitriding the plurality of iron particles to form the plurality of iron nitride nanoparticles further comprises forming the plurality of iron nitride nanoparticles comprising at least one of Fe_4N, $Fe_4N_xZ_{1-x}$, α"-$Fe_{16}N_xZ_{2-x}$ or α'-$Fe_8N_xZ_{1-x}$, where Z includes at least one of C, B, P, Si, or O based on introduction of at least one of carbon, boron, silicon, phosphorus, or oxygen to the furnace.

Example 8

[0086] The method of any of examples 1 through 7, wherein wet ball milling the plurality of iron nitride nanoparticles in the presence of a surface active agent comprises wet ball milling the plurality of iron nitride nanoparticles in the presence of a source of at least one of: polyvinylpyrrolidone, a polyoxyalkylene amine derivative, polyethylene glycol, ethylene glycol monobutyl ether, nonylphenol, or tetramethylammonium hydroxide.

Example 9

[0087] The method of any of examples 1 through 8, wherein wet ball milling the plurality of iron nitride nanoparticles in the presence of a surface active agent comprises wet ball milling for a period of between about 1 hour and about 10 hours at an rpm of between about 100 rpm and about 1000 rpm.

Example 10

[0088] The method of any of examples 3 through 9, wherein centrifuging the plurality of surface-modified iron nitride nanoparticles comprises centrifuging the plurality of surface-modified iron nitride nanoparticles at an rpm and for a time selected to obtain a set of surface-modified iron nitride nanoparticles having an average diameter of less than about 100 nm.

Example 11

[0089] The method of example 10, wherein centrifuging the plurality of surface-modified iron nitride nanoparticles comprises centrifuging the plurality of surface-modified iron nitride nanoparticles at a revolutions per minute (RPM) and

for a time selected to obtain a set of surface-modified iron nitride nanoparticles having an average diameter of less than about 50 nm.

Example 12

[0090] The method of any of examples 3 through 11, wherein centrifuging the plurality of surface-modified iron nitride nanoparticles comprises centrifuging the plurality of surface-modified iron nitride nanoparticles at an rpm and for a time selected to obtain a set of surface-modified iron nitride nanoparticles having unimodal size distribution.

Example 13

[0091] The method of any of examples 3 through 12, wherein centrifuging the plurality of surface-modified iron nitride nanoparticles comprises centrifuging the plurality of surface-modified iron nitride nanoparticles at a revolutions per minute (RPM) between about 1,000 RPM and about 50,000 RPM.

Example 14

[0092] The method of example 13, wherein centrifuging the plurality of surface-modified iron nitride nanoparticles comprises centrifuging the plurality of surface-modified iron nitride nanoparticles at an rpm of about 2,000 RPM or about 11,000 RPM.

Example 15

[0093] A suspension includes a solvent; and a plurality of surface-modified iron nitride nanoparticles suspended in the solvent.

Example 16

[0094] The suspension of example 15, wherein the plurality of surface-modified iron nitride nanoparticles have an average diameter of less than 100 nm.

Example 17

[0095] The suspension of example 16, wherein the plurality of surface-modified iron nitride nanoparticles have an average diameter of less than 50 nm.

Example 18

[0096] The suspension of any of examples 15 through 17, wherein the plurality of surface-modified iron nitride nanoparticles have a substantially unimodal size distribution.

Example 19

[0097] The suspension of any of examples 15 through 18, wherein the plurality of surface-modified iron nitride nanoparticles are surface-modified by at least one of polyvinylpyrrolidone, a polyoxyalkylene amine derivative, polyethylene glycol, ethylene glycol monobutyl ether, nonylphenol, or tetramethylammonium hydroxide.

Example 20

[0098] The suspension of any of examples 15 through 19, wherein the plurality of surface-modified iron nitride nanoparticles comprise at least one of γ'-Fe_4N, γ'-$Fe_4N_xZ_{1-x}$, α'-Fe_8N, α''-$Fe_{16}N_xZ_{2-x}$, or α'-$Fe_8N_xZ_{1-x}$, wherein Z comprises at least one of C, B, P, Si, or O.

Example 21

[0099] A soft magnetic material includes a plurality of consolidated surface-modified iron nitride nanoparticles, wherein the plurality of consolidated surface-modified iron nitride nanoparticles have an average diameter less than about 100 nm.

Example 22

[0100] The soft magnetic material of example 21, wherein the plurality of consolidated surface-modified iron nitride nanoparticles are dispersed in a binder.

Example 23

[0101] The soft magnetic material of example 21 or 22, wherein the plurality of consolidated surface-modified iron nitride nanoparticles have a substantially irregular shape.

Example 24

[0102] The soft magnetic material of any of examples 21 through 23, wherein the plurality of consolidated surface-modified iron nitride nanoparticles have a coercivity less than about 200 Oe.

Example 25

[0103] The soft magnetic material of any of examples 21 through 24, wherein the plurality of consolidated surface-modified iron nitride nanoparticles are surface-modified by at least one of polyvinylpyrrolidone, a polyoxyalkylene amine derivative, polyethylene glycol, ethylene glycol monobutyl ether, nonylphenol, or tetramethylammonium hydroxide.

Example 26

[0104] The soft magnetic material of any of examples 21 through 25, wherein the plurality of consolidated surface-modified iron nitride nanoparticles comprise at least one of γ'-Fe_4N, γ'-$Fe_4N_xZ_{1-x}$, α'-Fe_8N, α''-$Fe_{16}N_xZ_{2-x}$, or α'-$Fe_8N_xZ_{1-x}$, wherein Z comprises at least one of C, B, P, Si, or O.

[0105] Various examples have been described. These and other examples are within the scope of the following claims.

What is claimed is:

1. A method comprising:

wet ball milling a plurality of iron nitride nanoparticles in presence of a surface active agent to modify a surface of the plurality of iron nitride nanoparticles and form a plurality of surface-modified iron nitride nanoparticles.

2. The method of claim **1**, wherein the plurality of iron nitride nanoparticles comprise at least one of γ'-Fe_4N, α'-Fe_8N, α''-$Fe_{16}N_xZ_{2-x}$, or α'-$Fe_8N_xZ_{1-x}$, wherein Z comprises at least one of C, B, P, Si, or O.

3. The method of claim **1**, further comprising:

centrifuging the plurality of surface-modified iron nitride nanoparticles to separate a set of surface-modified iron nitride nanoparticles having a selected size profile from the plurality of surface-modified iron nitride nanoparticles.

4. The method of claim **1**, further comprising:

forming the plurality of iron nitride nanoparticles from a plurality of iron oxide nanoparticles using a gas phase nitriding process.

5. The method of claim 4, wherein the plurality of iron oxide nanoparticles comprise a plurality of γ-Fe_2O_3 nanoparticles.

6. The method of claim 4, wherein the gas phase nitriding process comprises:

reducing, in a furnace, the plurality of iron oxide nanoparticles to form a plurality of iron nanoparticles; and

nitriding the plurality of iron particles to form the plurality of iron nitride nanoparticles.

7. The method of claim 6, wherein nitriding the plurality of iron particles to form the plurality of iron nitride nanoparticles further comprises forming the plurality of iron nitride nanoparticles comprising at least one of Fe_4N, $Fe_4N_xZ_{1-x}$, α''-$Fe_{16}N_xZ_{2-x}$, or α'-$Fe_8N_xZ_{1-x}$, where Z includes at least one of C, B, P, Si, or O based on introduction of at least one of carbon, boron, silicon, phosphorus, or oxygen to the furnace.

8. The method of claim 1, wherein wet ball milling the plurality of iron nitride nanoparticles in the presence of the surface active agent comprises wet ball milling the plurality of iron nitride nanoparticles in the presence of a source of at least one of: polyvinylpyrrolidone, a polyoxyalkylene amine derivative, polyethylene glycol, ethylene glycol monobutyl ether, nonylphenol, or tetramethylammonium hydroxide.

9. The method of claim 1, wherein wet ball milling the plurality of iron nitride nanoparticles in the presence of the surface active agent comprises wet ball milling for a period of between about 1 hour and about 10 hours at an rpm of between about 100 revolutions per minute (RPM) and about 1000 RPM.

10. The method of claim 3, wherein centrifuging the plurality of surface-modified iron nitride nanoparticles comprises centrifuging the plurality of surface-modified iron nitride nanoparticles at a revolutions per minute (RPM) and for a time selected to obtain a set of surface-modified iron nitride nanoparticles having at least one of an average diameter of less than about 100 nm or a substantially unimodal size distribution.

11. The method of claim 3, wherein centrifuging the plurality of surface-modified iron nitride nanoparticles comprises centrifuging the plurality of surface-modified iron nitride nanoparticles at an rpm of about 2,000 revolutions per minute (RPM) or about 11,000 RPM.

12. A suspension comprising:

a solvent; and

a plurality of surface-modified iron nitride nanoparticles suspended in the solvent.

13. The suspension of claim 12, wherein the plurality of surface-modified iron nitride nanoparticles have an average diameter of less than 100 nm.

14. The suspension of claim 13, wherein the plurality of surface-modified iron nitride nanoparticles have an average diameter of less than 20 nm.

15. The suspension of claim 12, wherein the plurality of surface-modified iron nitride nanoparticles have a substantially unimodal size distribution.

16. The suspension of claim 12, wherein the plurality of surface-modified iron nitride nanoparticles are surface-modified by at least one of polyvinylpyrrolidone, a polyoxyalkylene amine derivative, polyethylene glycol, ethylene glycol monobutyl ether, nonylphenol, or tetramethylammonium hydroxide.

17. The suspension of claim 12, wherein the plurality of surface-modified iron nitride nanoparticles comprise at least one of γ'-Fe_4N, γ'-$Fe_4N_xZ_{1-x}$, α'-Fe_8N, α''-$Fe_{16}N_xZ_{2-x}$, or α'-$Fe_8N_xZ_{1-x}$, wherein Z comprises at least one of C, B, P, Si, or O.

18. A soft magnetic material, comprising:

a plurality of consolidated surface-modified iron nitride nanoparticles,

wherein the plurality of consolidated surface-modified iron nitride nanoparticles have an average diameter of less than 100 nm.

19. The soft magnetic material of claim 18, wherein the plurality of consolidated surface-modified iron nitride nanoparticles have a substantially irregular shape.

20. The soft magnetic material of claim 18, wherein the plurality of consolidated surface-modified iron nitride nanoparticles are dispersed in a binder.

* * * * *